

Single-cell RNA sequencing of spinal cord microglia in a mouse model of neuropathic pain

Alba Ureña Guzmán

Division of Experimental Medicine

McGill University, Montreal

October 2021

A thesis submitted to McGill University in partial fulfillment of the requirements of the degree of M.Sc. in Experimental Medicine

© Alba Ureña Guzmán, 2021

Table of Contents

Abstract	4
Résumé.....	6
List of figures.....	8
List of tables	9
Acknowledgements	10
Contributions	12
1. Introduction	13
1.1 Pain.....	13
1.1.1 Neuropathic pain.....	14
1.1.2 Transition from acute to chronic pain.....	15
1.1.3 Animal models of neuropathic pain.....	16
1.1.4 Pain processing in the spinal cord	20
1.1.5 Sex differences in pain processing	21
1.2.1 Functions of microglia in homeostasis and disease states	23
1.2.2 Heterogeneity of microglia in development, homeostasis, & disease mice....	25
1.2.3 Microglia in neuropathic pain	27
1.2.4 Gene expression for characterization of microglia	29
1.3 Rationale and aims	31
2. Methodology.....	33
2.1 Aim 1	33
2.1.1 Animals.....	33
2.1.2 Neuropathic pain model.....	33
2.1.3 Harvesting of microglia from dorsal horn of spinal cord	34
2.1.4 Single-cell RNA sequencing of mouse spinal cord microglia	35
2.1.5 Single-cell RNA sequencing data processing	36
2.1.6 GO ontology and pathway enrichment analysis.....	37
2.1.7 In situ hybridization and imaging.....	37
2.1.8 Immunohistochemistry (IHC) and imaging	38
2.1.9 Image analysis and quantification.....	39
2.1.10 Statistical analysis	40
2.2 Aim 2.....	40

2.2.1 Animals	40
2.2.2 Tamoxifen administration	40
2.2.3 Neuropathic pain model	41
2.2.4 Tissue clearance with X-CLARITY	41
2.2.5 3D image acquisition	42
2.2.6 Image processing and quantification	42
3. Results	43
3.1 Transcriptional landscape of spinal microglia at the single cell level after peripheral nerve injury	43
3.2 Sex-specific changes in the transcriptome of microglia after peripheral nerve injury	48
3.3 Peripheral nerve injury induces greater proliferation of microglia in the lumbar spinal cord of male mice as compared to female mice	54
3.4 Apoe is upregulated in spinal microglia at chronic phases of neuropathic pain ...	60
3.6 LYVE-1 positive cells are observed in the lumbar spinal cord in proximity to blood vessels	63
3.7 3D imaging of microglia using light-sheet microscopy	65
4. Discussion	70
4.1 Single-cell RNA sequencing of spinal microglia reveals transcriptional heterogeneity after peripheral nerve injury	70
4.2 Sex-specific changes in the transcriptome of microglia after peripheral nerve injury	72
4.3 Peripheral nerve injury induces greater proliferation of microglia in the lumbar spinal cord of male mice as compared to female mice	74
4.4 APOE is upregulated in spinal microglia at chronic phases of neuropathic pain ..	75
4.5 LYVE-1 positive cells are observed in the lumbar spinal cord in proximity to blood vessels	76
4.6 3D imaging of microglia using light-sheet microscopy	76
Conclusion	77
References	78
Appendix A	84
Appendix B	85
Appendix C	86

Abstract

Peripheral nerve injury (PNI)-induced activation and proliferation of microglia in the spinal cord contribute to the development of neuropathic pain. Microglia inhibition reverses mechanical allodynia after PNI only in male mice. To study the potential mechanisms by which microglia promote pain and investigate changes in their transcriptional states, we performed microglia single-cell RNA-seq following spared nerve injury (SNI) in male and female mice at different phases of pain development. Single-cell RNA-sequencing was performed on microglia isolated from the lumbar spinal cord of male and female naive C57BL/6 mice as well as mice of both sexes at day 3 (developmental phase), day 14 (early chronic phase), and 5 months (chronic phase) post-SNI and sham controls. Unsupervised clustering analysis of single-cell RNA sequencing data revealed eleven distinct microglia clusters. Gene ontology analysis identified clusters involved in proliferation, immune response, and signal transduction. Quantification of Ki67-positive microglia in the dorsal horn spinal cord three days post-SNI showed a significantly higher number of proliferating microglia in males, as compared to females, with no differences in the total number of microglia. We also identified a male-specific microglia cluster with an inflammatory profile restricted to early time points after injury. Apoe was found as the top upregulated gene in microglia at time points after nerve injury in mice in which chronic pain hypersensitivity has developed. Increased protein levels of Apoe were also found at late time points. LYVE1 / IBA1-positive cells were found in proximity to blood vessels in the mouse spinal cord. The function of these cells in the context of nerve injury remains to be explored. 3D imaging of cleared mouse lumbar spinal cord revealed different microgliosis patterns in males

and females 3 days post-SNI. Female microglia density increased similarly in the dorsal and ventral horns ipsilateral to the injury, whereas male microglia peaked first in the ventral horn and later in the dorsal horn. The results of this study provide evidence for sex-specific responses of microglia to peripheral nerve injury. Further research on the role of APOE in microglia and the function of LYVE1 / IBA1-positive cells in the mouse spinal cord might provide important insights into the mechanisms underlying neuropathic pain.

Résumé

La blessure neuropathie périphérique (BNP) contribue à l'activation et la prolifération des microglies dans la moelle spinale et celles-ci attribuent au développement de la douleur neuropathique. Inhibition des microglies inverse l'allodynie mécanique après BNP seulement dans les souris mâles. Pour étudier les mécanismes potentiels par lequel les microglies promouvaient la douleur et pour investiguer les changements dans leurs états transcriptionnels, nous avons utilisés le « single-cell RNA-seq » après « spared nerve injury (SNI) » dans les souris mâles et femelles dans des phases différentes du développement du douleur. Le « RNA-seq » a été fait sur les microglies isolées de la région lombaire de la moelle spinale des souris C57BL/6 mâles et femelles naïves, ainsi que des souris des deux sexes au journée 3 (phase développement), journée 14 (phase chronique plus tôt), et 5 mois (phase chronique) après le « SNI » et des contrôles « shams ». L'analyse rassemblant non-supervisé du data « RNA-seq » a révélé onze groupes distincts de microglie. L'analyse d'ontologie génétique a identifié des groupes impliquer dans la prolifération, la réponse immune, et la transduction des signaux. Quantification des microglies positives pour le Ki67 dans la corne dorsale de la moelle spinale trois jours après « SNI » a démontrée des nombres élevés significatifs de microglies proliférants dans les mâles, en comparaison que dans les femelles, ainsi qu'aucune différence dans le nombre total de microglie. Nous avons aussi identifié un groupe de microglie uniquement dans les mâles avec un profile inflammatoire qui est restreinte au temps plus tôt après la blessure. Apoe était le gène le plus haut-réglé dans les microglies des souris quand la blessure neuropathique a développée dans le douleur chronique hypersensitive. L'élévation des quantités de protéine d'Apoe a été

aussi retrouvé dans les temps plus tard. Des cellules positives pour le LYVE1 / IBA1 a été trouvé proche des vaisseaux sanguins dans la moelle spinale des souris. La fonction de ces cellules dans le contexte de la blessure neuropathique doit être exploré. L'image 3D des moelles spinales lombaires dégagées des souris a démontré différents motifs de microglie dans les mâles et les femelles 3 jours après le « SNI ». La densité de microglie dans les femelles a été élevée au même niveau dans les cornes dorsales et ventrales ipsilatérales de la blessure. Dans les mâles, la densité de microglie a été maximale dans la corne ventrale en première, et après dans la corne dorsale. Les résultats de cette étude fournissent l'évidence des effets spécifiques pour le sexe des microglies à cause de la blessure neuropathie périphérique. Plus de recherche sur le rôle d'APOE dans les microglies et le fonctionnement des cellules positives pour LYVE1 / IBA1 dans la moelle spinale des souris peuvent offrir des aperçus importants sur les mécanismes de la douleur neuropathique.

List of figures

Figure 1. Characterization of microglia at the single-cell level after nerve injury.	44
Figure 2. UMAP plot colored for the expression (log-normalized counts) of canonical microglial genes.	45
Figure 3. UMAP plot colored for the expression (log-normalized counts) of the top unique gene in the indicated microglial cluster.	46
Figure 4. Gene Ontology terms (biological process) enriched in markers from clusters 1-6, 7, 8 and 9.	47
Figure 5. GO analysis of microglia from naïve female and male mice.	50
Figure 6. Sex-specific changes in the transcriptome of microglia after peripheral nerve injury.	51
Figure 7. GO analysis of males and females after peripheral nerve injury.	53
Figure 8. The cell proportion varies across the different microglia clusters.	53
Figure 9. Peripheral nerve injury gives rise to a male-specific cluster of microglia.	54
Figure 10. Peripheral nerve injury changes the proportion of microglia belonging to the proliferating clusters.	55
Figure 11. Peripheral nerve injury induces greater proliferation of microglia in males as compared to females.	57
Figure 12. Peripheral nerve injury induces greater proliferation of microglia in males as compared to female <i>Tmem119CreERT2</i> ; <i>Ai14</i> mice.	58
Figure 13. Cleaved caspase-3 immunoreactivity in the spinal cord of a male mouse 3 days post-SNI.	59
Figure 14. Gene expression of <i>ApoE</i> is increased in microglia in chronic phases of neuropathic pain.	61
Figure 15. <i>ApoE</i> is increased in microglia in chronic phases of neuropathic pain.	62
Figure 16. LYVE1 positive cells in proximity to blood vessels in the mouse spinal cord.	64
Figure 17. Clearing and imaging of mouse spinal cord.	66
Figure 18. Fluorescently labeled microglia in the spinal cord.	67
Figure 19. 3D reconstruction of mouse lumbar spinal cord of <i>Tmem119cre^{ERT2/+}</i> ; <i>Ai14^{tdTomato/+}</i> mice.	68
Figure 20. Quantification of microglia in the lumbar region of cleared mouse spinal cord.	69

List of tables

Table 1. Top five upregulated genes per cluster.....	46
Table 2. Fold change of MAPK and inflammation related genes.	52
Table 3. Fold change (LogFC) of <i>ApoE</i> mRNA in females and males across time points and clusters.....	63

Acknowledgements

I would like to thank my supervisor, Dr. Arkady Khoutorsky, for allowing me to be part of the lab and the projects. His constant guidance and support have been the key to the fulfillment of my master's degree. Besides his guidance, he allows to experiment with new complicated techniques and pursue novel ideas. The dynamism in the techniques and fields of research makes the lab a favorable environment for learning.

I would like to thank my committee members, Dr. Ji Zhang, Dr. Jeffery Mogil, and my academic advisor Dr. Peter Siegel for their valuable feedback during the committee meetings.

I want to thank all the members of the Khoutorsky lab, Jieyi, Patricia, Weihua, Kevin, Calvin, and Mehdi, for their help, support, and patience these past two years, especially to Shannon and Sonali who welcomed me into their project and taught me everything. In addition, a thank you to Dr. Daneck Lang-Ouellette for training me on the X-Clarity system and the ABIF facility for their support with my imaging experiments, especially to Dr. Anne-Marie Ladouceur. Thanks to Manon St. Louise for her training on the use of the cryostat. I thank my former university professors and previous supervisors (Ana María Ibarra Humphries and Serge McGraw). Without them, I would not be here. I also thank the funding agencies that made my studies possible, the National Council for Science and Technology (CONACYT) and Mitacs.

Finally, I would like to thank my family, they are the most important part of my life, and I could not have finished my studies without them. My parents have always supported me in my decisions, while the rest of my family cheers me up when I need them. I'm lucky to

have amazing friends in Mexico and Montreal who would bring me up when experiments were not going well.

Especially, I want to dedicate this to my nana. Even though she could not understand how I worked with mice, she would have been at the graduation ceremony even if it was a -20°C.

Contributions

S. Tansley and S. Austin assisted with SNI and sham surgeries. S. Tansley, S. Uttam and A. Ureña Guzmán harvested animal tissue and prepared samples for single-cell RNA sequencing. A. Pacis performed the bioinformatics analysis on single-cell RNA sequencing data. A. Ureña Guzmán performed data mining, gene ontology and pathway analyses, RNA *in situ* hybridization experiments, immunohistochemistry studies, tamoxifen administration, tissue clearance, 2D and 3D imaging, image processing and quantification, and statistical analysis.

1. Introduction

1.1 Pain

The International Association for the Study of Pain (IASP) defines pain as ‘an unpleasant sensory and emotional experience associated with, or resembling that associated with, actual or potential tissue damage’.(1) It can be classified into three categories; nociceptive pain, inflammatory pain, and pathological pain, which is further divided into neuropathic pain and dysfunctional pain. The first two categories play a protective role, whereas the third one is maladaptive. Briefly, nociceptive pain is the pain that we feel when we are in contact with a noxious stimulus. It is the warning signal coming from our bodies that prevents us from getting hurt.(2) Inflammatory pain results from the release of inflammatory mediators (e.g. cytokines, bioactive molecules) following tissue injury or infection and has the purpose of preventing further damage and promoting the healing of an injured body part by inducing pain hypersensitivity that discourages moving the affected body part.(2) Pathological pain refers to the pain that continues after the injured body part has healed and it is characterized by an increased response to stimuli that are normally innocuous, namely allodynia, and by an augmented response to painful stimuli, called hyperalgesia.(3) Pathological pain results following damage of the nervous system in the case of neuropathic pain, but also without such damage or inflammation in dysfunctional pain, which can be triggered by conditions like irritable bowel syndrome or fibromyalgia.(2) In the following sections, we will address the key players involved in neuropathic pain.

1.1.1 Neuropathic pain

As of 2011, the definition of neuropathic pain is 'pain caused by a lesion or disease of the somatosensory system'.⁽⁴⁾ This includes neurons in the spinal cord as well as peripheral fibers: A β , A δ , and C fibers.⁽⁵⁾ Neuropathic pain is characterized by spontaneous pain, hyperalgesia, and tactile allodynia. Neuropathic pain has heterogeneous origins that include metabolic disorders, inflammatory disorders, autoimmune diseases affecting the CNS, neuropathies associated with viral infections, chemotherapy-induced peripheral neuropathies, hereditary neuropathies, channelopathies, and damage to the nervous system with a traumatic origin, like amputation or spinal cord injury.⁽⁶⁾ The lack of simple screening tools has made it difficult to measure the incidence and prevalence of neuropathic pain among the general population.⁽⁷⁾ Nevertheless, a systematic review of studies conducted from 1966 to 2012 in several European countries, USA, Brazil, Taiwan and Canada, estimated that the prevalence of pain with neuropathic characteristics affects about 6.9 to 10% of people.⁽⁷⁾ Women show a higher prevalence, constituting 60.5% of patients.⁽⁶⁾ Due to the complexity of its symptoms, neuropathic pain is difficult to treat, and there are poor outcomes, with a major impact on quality of life.⁽⁵⁾ Treatment of neuropathic pain patients does not provide adequate pain relief, likely because of an incorrect diagnose, inefficient drugs, or lack of knowledge regarding drugs in the clinical setting.⁽⁸⁾ In 2015, the Neuropathic Pain Special Interest group (NeuPSIG) of the IASP published the results of a systematic review of studies conducted from 1966 to April 2013 where it recommends tricyclic antidepressants, serotonin noradrenaline reuptake inhibitors, pregabalin, gabapentin and gabapentin ER/enacarbil as the first line of

treatment for neuropathic pain.(8) However, these drugs are often accompanied by side effects, to the point that satisfactory pain relief is not accomplished at tolerated doses.(9)

1.1.2 Transition from acute to chronic pain

Pain is usually classified as acute, tonic, or chronic. Acute pain refers to the rapid onset of a discomforting sensation on a defined location associated with a specific trauma or disease.(10) Chronic pain continues after the normal time for healing has passed and does not function as a warning signal, unlike acute pain. Pain is considered chronic when it lasts for more than three months. Chronic pain affects around 20% of the population worldwide.(11) The transition from acute to chronic pain results from maladaptive neuroplasticity, involving three connected processes: peripheral sensitization, central sensitization, and descending modulation.(12)

Peripheral sensitization results from the exposure of nociceptors to inflammatory mediators released following tissue injury.(10) The inflammatory process involves the activation of lymphocytes and the release of cytokines such as TNF- α , IL6, and IL1 β . Chronic inflammation causes several complex changes in the periphery that include: reduction in the pain threshold at nociceptive terminals, increased sensitivity, phosphorylation of protein kinases A and C, activation of the transient receptor potential vanilloid (TRPV) receptors via phosphorylation, up-regulation of TRPV1, and voltage-gated sodium channels in the dorsal root ganglion (DRG), and increased production of CGRP(Calcitonin gene-related peptide) and substance P in both the periphery and spinal cord.(13)

In central sensitization, second and third-order neurons constantly increase their reaction to repeated nonpainful stimuli, and even develop spontaneous activity.(12) The continuous input from nociceptors leads to an increased expression of several receptors and ion channels in dorsal horn neurons, such as sodium channels, TRPV1, and N-methyl-D-aspartate (NMDA) receptors, that results in the hyperexcitable state.(13) Similar to peripheral sensitization, cytokines and neuropeptides are released at the level of the spinal cord. Repeated activation of nociceptors induces the release of neurotransmitters like CGRP, substance P, glutamate, and ATP, neuronal chemokines such as fractalkine and monocyte chemoattractant protein-1, and neuromodulators including prostaglandins and NO(Nitric oxide) (13), acting via different mechanisms to enhance the excitability of spinal cord nociceptive circuits.

Imaging studies in humans and animals have shown that the duration of pain is influenced by descending pathways that involve different regions including the thalamus, periaqueductal gray, rostroventral medulla, nucleus caudalis, reticular formation, mid/anterior insula, anterior cingulate cortex, and prefrontal cortex.(12, 13)

1.1.3 Animal models of neuropathic pain

Several models of neuropathic pain have been developed with the goal to identify the molecular and cellular mechanisms underlying this type of pain.(14) The use of animal models over human subjects presents several advantages. Animal models allow the standardization of genetic and environmental backgrounds, the analysis of specific tissue, and the characterization of anatomical, neurochemical, and electrophysiological properties, besides its safety and low-cost.(15) It is difficult to employ humans in this type of research, given that the stimulus needed to induce neuropathic pain usually

leads to irreversible damage.(16) It would be unthinkable to apply models with, for example, partial denervation in humans. Using actual patients adds confounding factors that make the analysis of experimental data difficult.(15) Furthermore, gathering large numbers of participants for this type of study is a complicated task.(16)

In the 1980s, most of the animal models of neuropathic pain were designed and conducted in rats. However, the development of transgenic mouse lines has tremendously promoted the use of mice, going from ~60 articles published in 1995 to ~300 in 2017, while papers on rats increased from ~200 to ~700 in the same period.(14, 17)

Numerous neuropathic pain models have been designed to recapitulate pain conditions observed in clinical setting, which arise from different etiology. There are several widely used models to study neuropathic pain.(16) Peripheral nerve injury models include chronic constriction injury, partial sciatic nerve ligation, spinal nerve ligation, spared nerve injury (SNI), the axotomy model, etc. Central pain models comprise excitotoxic spinal cord injury, photochemical spinal cord injury, weight drop, and spinal hemisection.(16) Drug-induced neuropathy models involve anti-HIV drugs and anti-cancer agents such as taxanes, platinum compounds and vincristine. Disease-induced neuropathy models include diabetes, cancer, HIV, and post-herpetic neuralgia.(16)

The SNI model consists of the cut and ligation of the tibial and common peroneal nerves (two of the three-terminal branches of the sciatic nerve), leaving the sural nerve intact. It is a model that rapidly (<24 hrs) induces robust behavioral effects lasting for more than six months. The mechanical and thermal sensitivity is increased in the ipsilateral sural territory.(18) SNI recapitulates several clinical features of neuropathic, it is relatively

easy to perform and shows less variability in the nerve damage.(16) However, it is difficult to assess pain behavior in SNI animals given that the ipsilateral paw has uninjured regions close to the denervated areas, and the hypersensitivity is on the lateral part of the paw, which is technically challenging to evaluate.(19)

There has been moderate success in the transition from experimental data gathered in animal models to safe and effective pain medication, in part, because of adverse side effects and lack of efficacy in human subjects.(17) As an example, in human trials of several clinical pain states, neurokinin-1 (NK1) antagonists did not show the efficacy that was predicted from animal models.(20) The limited translation of scientific data into the clinic could be the result of inadequate models, subjects that are being used in preclinical studies, outcome measures, or the experimental design.(21)

Most animal models on neuropathic pain rely on traumatic injury to a nerve, usually the sciatic.(22) However, this is not the case in the clinical setting where trials conducted on patients with peripheral nerve injuries represent only 9% of the trials; in comparison, trials on patients with peripheral polyneuropathies and post-herpetic neuralgia comprise 53% and 21%, respectively.(21) Special consideration should be address to the subjects used in the preclinical studies since differences in the laboratory animals, strain, and age influence the development of pain behavior.(21) The different tests used to evaluate the outcome measures of pain research, such as spontaneous pain, hypersensitivity, and comorbidities, could give insights into the pathophysiology of the pain state and the effects of new drugs.(21)

Pain sensation in animals is inferred from “pain-like” behaviors, including withdrawal from a nociceptive stimulus, limited ambulation, vocalizations, agitation, and increased

grooming.(23) Indeed, the most frequently used test to measure nociception in animals is withdrawal from a stimulus.

Behavioral tests can be divided into reflexive or non-reflexive tests. In reflexive pain tests, an external stimulus (heat, cold, mechanical, or electrical) is applied to measure evoked behavioral responses. These tests activate the nociceptors located at site where the stimulus is applied, and normally, the response does not involve supraspinal activation.(24) On the contralateral side, non-reflexive tests do not require any stimuli. Reflexive tests used in animal models of neuropathic pain include the hot plate test and Hargreaves test for heat stimuli, acetone or dry ice tests for assessment of cold sensation, and Randall-Selitto test and manual or electronic von Frey for mechanical stimuli.(24) Among non-reflexive tests are Mouse Grimace Scale(MGS), conditioned place preference and escape/avoidance tests. The MGS is a standardized behavioral coding system that can be used for pain assessment in the laboratory or veterinary settings and measures the spontaneous pain behavior emitted by the subject as facial expressions in the absence of an experimenter.(25)

The measurement in most behavioral tests is to some extent subjective. For example, a researcher could determine that the animal withdrew its limb following the stimuli due to its aversive nature or for a different motive like grooming. Besides, behaviors in tests are measured as present or absent, while in reality, they occur as a spectrum.(23) As mentioned before, the most frequently used test to measure nociception is withdrawal from a stimulus. However, neuropathic pain patients predominantly suffer from spontaneous pain, and mechanical hypersensitivity is only present in 57% of patients

and thermal hypersensitivity in 33%.⁽²¹⁾ This calls for a careful experimental design in order to increase the probabilities of translating the research into the clinic.

1.1.4 Pain processing in the spinal cord

Nociceptive signalling consists of three events: transduction, transmission, and modulation. Transduction takes place when the noxious stimulus is converted to chemical and electrical signals, transmission happens when the electrical signals pass from one neuron to another, and modulation occurs along the entire pathway, from the first cell that signals the noxious stimulus to the spinal cord dorsal horn, and brain structures by up- or downregulation.⁽²⁶⁾

The detection of intense mechanical, thermal, or chemical stimuli is called nociception, and it is carried out by a subpopulation of peripheral nerve fibers, referred to as nociceptors.⁽²⁷⁾ Nociceptors transform information encoded by noxious stimuli such as pressure, heat, extreme cold, and chemicals into electrical activity.⁽²⁸⁾ Primary sensory neurons differ in the neurotransmitters they release, the receptors and ion channels they express, their capacity to be sensitized, the conduction speed, and their response to distinct stimuli.⁽²⁹⁾ Sensory neurons are divided into two general classes: the myelinated A-fibers and the unmyelinated C-fibers. A-fibers comprise the A δ fibers of medium-diameter cell bodies that mediate acute, well-localized fast pain, and the A β fibers of large-diameter that rapidly respond to non-noxious mechanical stimulation like light touch and therefore are not nociceptors.⁽²⁷⁾ C-fibers constitute approximately 70% of all nociceptors and mediate the slow, poorly localized pain. They have small diameter cell bodies and exhibit slow conduction of actions potentials along their axon.⁽²⁹⁾ C-fibers are also divided into two categories, peptidergic and nonpeptidergic. The former

contains several neuropeptides like substance P and calcitonin gene-related peptide (CGRP) and expresses trkA receptors, whereas nonpeptidergic fibers contain fewer neuropeptides and bind to the IB4 isolectin.(29) Nociceptors have four elements, a peripheral terminal that transduces diverse stimuli, an axon that carries action potentials toward the central nervous system (CNS) coming from the periphery, a cell body in the dorsal root or trigeminal ganglia, and a central axon that goes into the CNS and forms synapses with second order nociceptive neurons located in the spinal cord.(30) Axons coming from primary afferent nociceptors project to the different laminae in the dorsal horn of the spinal cord. A δ -fibers project to lamina I and V, A β -fibers to deep laminae III, IV, and V, and C-fibers to superficial laminae I and II.(27) Several ascending pathways connect the output from the integration and processing happening in the spinal cord dorsal horn to different regions in the brain.(28) The lateral spinothalamic tract projects multimodal sensory inputs and mainly carries information on pain (location and intensity) and temperature sensation towards the thalamus, while the anterior spinothalamic tract targets touch and firm pressure sensation.(26) The medial spinothalamic tract and the spinoparabrachial tract carry information to the medial thalamus and limbic structures to process the emotional and aversive properties of pain.(28)

1.1.5 Sex differences in pain processing

Several studies have revealed differences in the responses to pain across sexes, including prevalence, risks, and sensitivity. For example, the prevalence of chronic pain in women is ~6% higher than in males.(31) A study conducted in 2012 with medical records from more than 11,000 patients reported higher clinical pain scores in women

than in males, in multiple diseases, including osteoarthritis, arthropathies, and disorders of the back.(32) Differences in the responses to medication and non-pharmacological pain interventions have also been found, but the results are not conclusive. Although higher pain sensitivity in women in comparison to men is consistent across multiple pain measurements and stimulus modalities, the magnitude of the sex variation differs across studies.(33) The mechanisms underlying these differences between sexes take place at the 'genetic, molecular, cellular, and systems-level' of pain processing, in both rodents and humans.(34)

At the genetic level, sex differences seem to be influenced by the strain of the mouse or rat used for the study. A relationship between strain and sex has been shown for thermal nociception, mechanical allodynia after nerve injury, morphine tolerance, estrous cycle effects, gonadectomy effects, and opioid, non-opioid, and endogenous analgesia.(35) The role of individual genes in pain processing has been shown to have sex-specific effects in mice, as in the case for *Esr1*, *Esr2*, *Tlr4*, *P2rx7*, *Mc1r*, *Oprm1*, etc.(35) Polymorphisms of the OPRM1 gene also showed differences in pressure and heat pain sensitivity in humans.(36) The *MC1R* genotype in humans shows sex differences in the kappa-opioid analgesic response as well.(37) A review of studies conducted between 1966 and 1998 found that women consumed fewer opioids (self-administered) to manage postoperative pain.(38) However, this result has not been consistent across surgical procedures, and the studies measuring drug consumption instead of pain relief could mask the true response to medication, often influenced by side effects.(33)

Noticeable research supports that sex hormones influence pain sensitivity, which can be expected given the location of their receptors in both the peripheral and central nervous systems in regions associated with nociception.(33) Further studies are required to explain the contribution of sex hormones in pain processing. In further sections, we will discuss the significant sex differences found in the contribution of the immune system in the mediation of pain.

1.2 Microglia

Microglia are the resident immune cells in the CNS. They were discovered in 1932 by Pio del Rio-Hortega, who also introduced the term “Microglia”.(39) Microglia are derived from primitive myeloid progenitors that originate in the yolk sac at embryonic day 7 in mice.(40) Microglia are self-renewed, which is accomplished by coupled proliferation and apoptosis, maintaining a relatively steady number of cells throughout the organism’s lifetime without contribution from bone-marrow-derived monocytes.(41, 42) These cells migrate into the brain parenchyma and spinal cord and adopt a specific morphological phenotype.(39) In normal conditions, microglia display a ramified morphology, which changes into an amoeboid shape upon pathology.(43) Even though the cell body of microglia is static, these cells can survey their surroundings in areas bigger than ten times their soma and interact with neighboring cells, including neurons, astrocytes, and oligodendrocytes.(44)

1.2.1 Functions of microglia in homeostasis and disease states

Microglia have several functions in the CNS, depending on the age of the individual, the region of the CNS, and the state of the organism (in health or disease state).

Under steady-state conditions, microglia survey their environment searching for damage or infection signals and aid by migrating to the site if injury, proliferating and phagocytosing apoptotic cells or deposited proteins, and releasing different molecules like neurotrophins and cytokines to protect and maintain homeostasis.(45)

During development, microglia modulate neuronal circuitry in the brain and have an active role in synaptic pruning by removing the excess of synapses.(46) Microglia also remove synapses in the mature brain, contributing to neural plasticity.(47) In both development and adulthood, microglia interact with neural precursor cells (NPCs).

Although microglia regulate the number of NPCs by phagocytosing apoptotic NPCs, it has been shown that microglia also support neurogenesis by assisting in the proliferation, maturation, and survival of NPCs and neurons.(46)

During aging and disease states, microglia can become reactive or impaired in the different functions they play. Microglia contribute to disease states via their diverse roles in mediating synaptic maintenance and plasticity, excitotoxicity, oxidative stress, and inflammation. Any disruption in the CNS can trigger microglia "activation", a state where microglia migrate to the site of injury, proliferate, release beneficial or detrimental substances to their surroundings and phagocytose cells.(39) Persistent microglia activation was documented in different pathological conditions, including neurodevelopmental disorders, psychiatric disorders, traumatic injuries, tumor development, infectious diseases, and neurodegenerative diseases.(43) As previously mentioned, microglia play a role in several neurodegenerative diseases, such as Alzheimer's disease, multiple sclerosis, prion disease and amyotrophic lateral sclerosis.(48)

1.2.2 Heterogeneity of microglia in development, homeostasis, & disease mice

Microglia heterogeneity can be determined based on morphology, cell density, and expression of cellular markers. The classification of microglia morphology is related to the activation state. Under physiological conditions, “resting” microglia show high motility and a ramified morphology used to survey the environment. Additionally, they display a small, round cell body and numerous branching processes.(49) Following the detection of potentially dangerous molecules or abnormal signaling coming from the surrounding neurons and glial cells, microglia change their morphology and function into an activated state. These “activated” microglia show an amoeboid shape, a round cell body with fewer short and thick processes that allows them to move promptly to the site of injury, release cytotoxic substances and phagocyte cells or debris.(49)

The activation of microglia also gives rise to so called M1/M2 phenotype. The nomination M1/M2 for activated macrophages comes from the similarity found in helper T cells where Th1 and Th2 correspond to cells that secrete different cytokines.(50)

Upon injury, microglia and infiltrating macrophages adopt a pro-inflammatory (M1) phenotype after exposure to inflammatory cytokines like IFN- γ and TNF- α , pathogens, and cellular debris. M1 microglia release pro-inflammatory cytokines such as TNF- α , IL-1 β , and IL-12, besides antigen presentation and high expression of inducible NO (iNOS).(51) The alternative activation state (M2) results following exposure to IL-4. M2 microglia express anti-inflammatory cytokines, including IL-4, IL-10, IL-13, and TGF- β , and have a role in tissue remodeling, inflammatory dampening, immunoregulation, parasite clearance, angiogenesis, allergy response, and tumor promotion.(51)

Nonetheless, the classification of microglia as M1 and M2 has been criticized because it

was not supported by research findings, and it was adopted to simplify the interpretation of data in an era before the ontogeny and functions of microglia had been determined.(52) Instead, factors such as transcriptomic and proteomic profile, sexual dimorphism, regional heterogeneity, and response to different stimuli (e.g., infection, inflammation, traumatic injury) should be considered when defining microglia terminology.(52)

Although there are studies suggesting spatial heterogeneity of microglia, the current consensus is that the heterogeneity is rather limited across distinct regions of the CNS.(41) Further studies will be needed to answer this question.

Several studies report differences in microglia's number, morphology, and gene expression between male and female mice. Schwarz et al. found that the number and morphology of microglia vary across sexes, developmental state, and brain region, with males showing higher numbers of microglia in postnatal development and females having more amoeboid microglia later in development and throughout adulthood.(53) Weinhard et al. also reported sex differences in the volume of microglia and phagocytic activity during the first four postnatal weeks.(54) Using single-cell RNA sequencing (scRNAseq) technology, Hammond et al. found only minor sex differences in gene expression during development and homeostasis.(55) However, work of Villa et al. revealed significant sex differences in the adult transcriptome.(56) I will further discuss this matter in the following sections.

Microglia are highly heterogeneous at embryonic and early postnatal times.(55) Hammond et al. identified a subpopulation of microglia at embryonic day 14.5 (E14.5) that uniquely express membrane-spanning 4-domains, subfamily A, member 7 (*Ms4a7*),

along with *ApoE*, *Ccr1*, *Ms4a6c*, and *Tmem176a* as top markers, and show a transcriptional profile similar to brain border macrophages.(55) Masuda et al. also found embryonic clusters that expressed lysosome-related genes such as cathepsin B (*Ctsb*), cathepsin D (*Ctsd*), and lysosomal-associated membrane protein 1 (*Lamp1*).(57) Upon pathology, microglia also display distinct phenotypes. One example is the disease-associated microglia (DAM) subtype identified by Keren-Shaul et al. in an Alzheimer's model. These DAM phagocytic cells are conserved in mice and humans and show high expression levels of *Lpl*, *Itgax*, *ApoE*, and *Cst7*.(58) After lipopolysaccharide (LPS) injection, which is often used as a model of systemic inflammation, another context-dependent subtype of microglia was found. These activated microglia differed from the DAM subtype; genes including *Trem2*, *Tyrobp*, *Ctsd*, and *Hif1a* were downregulated following LPS injection but upregulated in DAM.(59) Different demyelination models (by administration of a copper chelating toxin cuprizone, injection of lysolecithin (LPC), and experimental autoimmune encephalomyelitis (EAE)) also revealed characteristic transcriptional profiles that differ from the previously described.(55, 57, 60) All these studies indicate that microglial diversity in gene expression is influenced by the perturbation of their environment determined by different pathologies.(41)

1.2.3 Microglia in neuropathic pain

Since the 1970s, the proliferation of non-neuronal cells in the spinal cord dorsal horn after peripheral nerve injury was consistently reported as well as a correlation between the activation of microglia and pain behavior.(61) In 2003, different groups showed a causal role of microglia in neuropathic pain, including the work of Tsuda et al. Using a

model of neuropathic pain (injury to the fifth lumbar spinal nerve in rats), they showed that nerve injury leads to the upregulation of the ATP receptor subtype P2X4 exclusively in microglia and that it is required for the development of tactile allodynia after nerve injury.(62) Even more, activation of P2X4Rs in microglia is sufficient to produce tactile allodynia in naive animals, and its inhibition attenuates mechanical allodynia.(62)

Similarly, Ji et al. showed that p38 mitogen-activated protein kinases (p38 MAPKs) were activated and upregulated in microglia after peripheral nerve injury, and their inhibition reduced the injury-induced mechanical allodynia.(63)

Following nerve injury, different molecules are released from damaged primary afferents, including Neuregulin-1, the chemokine (C-C motif) ligand 2 (CCL2), matrix metalloproteinase (MMP)-2 and MMP-9, and fractalkine, which cause changes in the morphology, migration, and enhanced proliferation of microglia.(64) Similarly, peripheral nerve injury induces the expression of colony-stimulating factor 1 (CSF1) in injured neurons. CSF1 is transported to the spinal cord, where it binds to its receptor on microglia and activates a DAP12-dependent pathway that further leads to the activation of genes related to pain hypersensitivity such as *Irf8* and *Irf5*; IRF5 binds to the *P2rx4* promoter to upregulate P2X4R expression in microglia.(65) Numerous studies have shown upregulation of microglia signaling molecules after peripheral nerve injury, including TNF, IL-18, TREM2 and CX3CR1, that positively contribute to mechanical allodynia, proving the involvement of microglia in the pathogenesis of neuropathic pain.(66)

Differences between males and females have been found in the pathogenesis of neuropathic pain and the role of microglia. Sorge et al. showed that Toll-like receptor 4

(TRL4), which is primarily expressed by microglia, mediates pain hypersensitivity exclusively in males in the SNI model of neuropathic pain.(67) Sorge et al. also found that mechanical pain hypersensitivity in female mice is not dependant on microglia. They transiently depleted microglia by injection of saporin toxin conjugated to macrophage antigen complex-1, the integrin CD11b/CD18 receptor, and reported similar microglial depletion in both males and females, but it resulted in the reversal of allodynia after SNI only in male rodents.(68) Additionally, intrathecal administration of minocycline (an inhibitor of glial function), TNP-ATP (P2X inhibitor), SB203580 (p38 MAPK inhibitor), and Y1036 (NGF/BDNF inhibitor) blocked allodynia induced by SNI exclusively in males, with no effect in female mice.(68) Taves et al. also showed that intrathecal injection of the p38 inhibitor skepinone reduced mechanical allodynia only in male mice and rats 7 days after chronic constriction injury, but not in females, regardless of similar microgliosis and expression of IBA-1 and CX3CR1 in both sexes.(69) Similarly, metformin impedes the development of neuropathic pain after SNI and reverses the activation of microglia exclusively in male rodents.(70)

1.2.4 Gene expression for characterization of microglia

The most generally used markers of microglia are ionized calcium-binding adapter molecule 1 (IBA-1), cluster of differentiation receptors (CD68, CD11b, CD14, CD45, CD80, and CD115), fractalkine receptor (CX3CR1), ferritin, F4/80, high-affinity immunoglobulin epsilon receptor subunit gamma (FCER1G) and vimentin. However, most of those markers are also present in other cells, like IBA-1 and CD68 in infiltrating macrophages, making the discrimination of microglia *in situ* difficult.(49) To date, the most specific microglial markers are transmembrane protein 119 (TMEM119) and

purinergic receptor P2Y₁₂R, which are not expressed in other immune cells, Ly6C monocytes, or organ-specific macrophages.(71) It has been shown that TMEM119 contributes to osteoblast differentiation and bone development.(72) However, its function in microglia remains unknown.

1.2.4.1 Single cell RNA sequencing of mouse microglia

In the past decade, bulk RNAseq technologies have been used to study gene expression patterns. The development of single-cell RNAseq allows the profiling of gene expression at the single-cell level, providing the necessary tool to investigate biological questions of cell heterogeneity and embryonic development, in contrast to bulk RNAseq that presents the averaged gene expression over thousands of cells.(73)

Single-cell RNAseq protocols start with the isolation of individual cells. There are several methods to isolate cells, including limiting dilution, micromanipulation, laser capture microdissection (LCM), microfluidics, magnetic-activated cell sorting (MACS), and fluorescence-activated cell sorting (FACS).(73) FACS requires large starting volumes of over 10,000 cells in suspension, and the samples must express fluorescent proteins or be stained with either fluorescent dyes or fluorescently conjugated antibodies.(74)

In previous sections, we mentioned studies that employed scRNAseq of microglia. Hammond et al. sequenced 76,000 mouse microglia during development, aging, and following brain injury. To isolate single microglia, they employed FACS using the markers CD45^{low}, CD11B^{high}, and CX3CR1^{high}.(55) Masuda et al. characterized microglial subpopulations from various regions of the CNS during development and disease, such as demyelinating and neurodegenerative diseases. The gating strategy

for FACS captured CD45^{int}CD11b⁺, Ly6C⁻Ly6G⁻, and CD206⁻ cells.(57) Li et al. also looked at microglia from different brain regions of embryonic, early postnatal, and adult mice, using CD45^{low}CD11b⁺ for sorting.(75) Keren-Shaul et al. discovered a disease-associated microglia subtype in a mouse model of Alzheimer's disease after sequencing 8,016 cells. Samples were gated for CD45⁺, CD11B⁺ and CD11C⁺.(58)

1.2.4.2 Sex differences in microglia transcriptomics

Although some studies have found only minor sex differences in microglia, Villa et al. isolated brain microglia from healthy adult male and female mice and uncovered significant differences in the transcriptomes.(56) They also showed a neuroprotective phenotype in female microglia that was maintained even after transfer into male mouse brains.(56) Furthermore, Guneykaya et al. found differences in the structure, function, transcriptomic, and even proteomic profiles of male and female microglia.(76) Microglia in males are located in specific areas of the brain, have a higher antigen-presenting capacity as compared to females, and also respond stronger to stimuli such as ATP, given the increased protein expression of purinergic receptors and higher baseline outward and inward currents.(76)

1.3 Rationale and aims

Most basic research on microglia's contribution to the generation of pain employed male subjects.(77) However, the Mogil lab first found sex differences in pain processing between male and female rodents.(67-70) Hence, it is essential to include both sexes when studying the underlying mechanisms of neuropathic pain development and maintenance. Because of the multiple and important roles of microglia in the CNS immune system, many studies have investigated microglia's transcriptional states and

found that these cells have transcriptionally distinct subpopulations in health and disease(55, 58) and between sexes.(56, 76) Likely, several microglial subpopulations are also found in the spinal cord. Therefore, the first aim of this study was to identify the transcriptional states of spinal microglia in male and female mice in response to peripheral nerve injury. To do this, we used single-cell RNA sequencing of microglia extracted from mice that underwent SNI, a model of neuropathic pain, as well as immunohistochemistry. Additionally, we aimed to evaluate microgliosis in the spinal cord after SNI in male and female mice employing tissue clearing techniques coupled with light-sheet microscopy. We hypothesized that microglia acquire different transcriptional states with specific spatial and temporal distribution in response to nerve injury that show differences between sexes. Lastly, we propose that the mechanisms underlying spinal microgliosis after peripheral nerve injury in the SNI model differ between male and female mice.

2. Methodology

2.1 Aim 1

2.1.1 Animals

C57BL/6J mice (8-12 weeks of age) of both sexes were obtained from The Jackson Laboratory (Bar Harbor, ME, USA). Male and female mice (6-12 weeks of age) were used in the study. Mice were housed at McGill University animal facility in standard shoebox cages with a maximum of 5 mice per cage, in a temperature-controlled environment on a 12-hour dark-light cycle (lights on at 07:00 h). Food (Envigo Teklad, 8604) and water were available *ad libitum*. Cages were changed on a weekly basis to maintain a clean environment. All mouse experiments were approved by the Animal Care Committee at McGill University and complied with Canadian Council on Animal Care guidelines.

2.1.2 Neuropathic pain model

For the single-cell RNA sequencing of microglia, mice were anesthetized with isoflurane (1.5%) and subjected to bilateral spared nerve injury (SNI) or sham surgeries. Bilateral surgeries were used to avoid dissection of the spinal cord into the ipsilateral and contralateral sides, which could increase variability and introduce artifacts in the sequencing data. In the case of RNA *in situ* hybridization and immunohistochemistry experiments, mice underwent unilateral surgeries. SNI surgeries were performed as previously described.⁽⁷⁸⁾ Briefly, the sciatic nerve was exposed after making an incision on the skin and the biceps femoris muscle of the mouse. Then, the tibial and common peroneal nerves (two of the three terminal branches of the sciatic nerve) were tightly

ligated with 7.0 silk (Covidien, S-1768K). Approximately 2 mm of each distal nerve were removed. The remaining sural nerve was left intact. For the sham surgeries, the sciatic nerve, with its three branches, was exposed but not ligated or transected. The muscle and skin were closed in separate layers using coated Vicryl (Ethicon, J489G).

2.1.3 Harvesting of microglia from dorsal horn of spinal cord

Fresh lumbar spinal cord samples were collected 3 days, 14 days and 5 months post-SNI or sham surgeries, as well as naïve mice from both sexes. One biological sample consisted of four pooled lumbar segments. The suspension of single microglia cells was adapted from Hammond et. al.(55) Mice were anesthetized and perfused via transcardial route with ice-cold Hank's balanced salt solution (HBSS). The spinal cords were extracted by inserting a 20G needle at the caudal end of the vertebral column with 3 mL of HBSS. The lumbar section of the spinal cord (~5 mm) was dissected and placed into well plates with 2 mg ml⁻¹ collagenase type IV (Gibco) in 3 ml DMEM. Using scissors, the cords were minced and then treated with 1 µl of DNase I (Thermo Scientific) for 45 min at 37°C. After 20 min into the incubation, the tissue was Dounce homogenized with pestle A 20 times and simultaneously rotated the pestle. The cell suspensions were passed through a 70 µm cell strainer pre-wet with DMEM and transferred to a prechilled 50 mL tube, followed by centrifugation at 22°C for 10 min (400 vcf, acceleration: 2, brake: 1). After decanting the supernatant, the same centrifugation parameters were used to wash the samples with 15 mL HBSS. Again, the supernatant was discarded, and the cell pellets resuspended in 13 mL of 30% Percoll (Sigma) diluted in room temperature HBSS. The cell suspension was deposited in a 15

mL tube, and 2 mL of HBSS were added. It was centrifuged for 20 min at 22°C (400 vcf, acceleration: 1, brake: 0). The cell debris and Percoll were carefully removed without disturbing the pellet at the bottom of the tube. The cell pellet was washed with 15 mL of ice-cold HBSS and centrifuged for 7 min at 4 °C (500 vcf, acceleration: 2, brake: 1). The HBSS was removed from the tubes, and the samples were resuspended in 500 µl of ice-cold FACS buffer (0.4% BSA (nonacetylated) in 1x PBS, sterile) with CD11b (PE), CD45 (APC-Cy7), and CX3CR1 antibodies from Biolegend at a 1:200 dilution, and kept for 1 hour on ice and protected from light. Samples were washed in 14 mL of ice-cold HBSS and centrifuged for 7 min at 4 °C (500 vcf, acceleration: 2, brake: 1). Finally, the supernatant was carefully removed, and the pellet was resuspended in 500 µl of ice-cold FACS buffer. The samples were kept on ice and protected from light until sorting. Samples were sorted using either a FACSAria III cell sorter (BD Biosciences) equipped with 405 nm, 488 nm, and 640 nm lasers and the appropriate filters or a FACSAria Fusion (BD Biosciences) equipped with a 405 nm, 488 nm, 561 nm, and 633 nm lasers and the appropriate filters. Live, single CD11b+, CD45 low, CX3CR1+ cells were sorted using a 70 µm nozzle at 70 psi. Gates were determined using fluorescence minus one sample.

2.1.4 Single-cell RNA sequencing of mouse spinal cord microglia

Approximately, 8,700 cells per sample were loaded into a Chromium Single Cell Chip (10x Genomics). The Chromium Single Cell 3' Library & Gel Bead Kit v3 (10X Genomics) was used for reverse transcription and library preparation, following the manufacturer instructions. Samples were sequenced on an Illumina NovaSeq

sequencer to an average depth of 43,000 reads per cell. Cell Ranger (v.3.0.1) (10X Genomics) was used for sample demultiplexing, barcode processing, unique molecular identifiers filtering, gene counting, and sample mapping to the reference transcriptome (mouse mm10 v.1.2.0).

2.1.5 Single-cell RNA sequencing data processing

Raw sequencing data for each sample was converted to matrices of expression counts using the Cell Ranger software provided by 10X Genomics (version 3.0.2). Briefly, raw BCL files from the Illumina HiSeq were demultiplexed into paired-end, gzip-compressed FASTQ files using Cell Ranger's *mkfastq*. Using Cell Ranger's *count*, reads were aligned to the GRCm38 (mm10) mouse reference genome, and transcript counts quantified for each annotated gene within every cell. The resulting UMI count matrices (genes x cells) were then provided as input to Seurat suite (version 3.1.0). To filter out low-quality cells, we defined a window of a minimum of 500 and a maximum of 4000 detected genes per cell. Cells with more than 5% of the transcript counts derived from mitochondrial-encoded genes were further removed.

To identify sex-mediated differences in response to injury, all microglia samples were merged and analyzed using reciprocal principal component analysis (PCA) with reference-based integration as part of the Seurat single-cell analysis package 43,44. Here we specify one or more of the datasets as the 'reference' for integrated analysis, with the remainder designated as 'query' datasets. In short, PCA was performed separately for each dataset, following normalization, variable feature selection, and scaling. Integration anchors were identified using both male and female naïve samples

as reference (*FindIntegrationAnchors* function with parameter *reduction* = “rpca”).

Clustering and visualization of the integrated dataset were performed using Uniform Manifold Approximation and Projection (UMAP), with the first 15 principal components at a resolution of 0.3. Differential expression analysis between two conditions was performed using *FindMarkers* with parameter *min.cells.group* = 20 (minimum of 20 cells in any group being compared). Differentially expressed genes were identified using the cutoffs: $|\log \text{fold-change}| > 0.25$ and Benjamini-Hochberg FDR < 0.05. Cluster-specific marker genes were identified using similar cutoffs (*FindAllMarkers* function; up-regulated genes only).

2.1.6 GO ontology and pathway enrichment analysis

Gene ontology (GO) for biological process and molecular function, as well as KEGG pathway enrichment analysis, was conducted using EnrichR(79-81), a web-based tool, with gene identities of the top 40 genes per cluster either upregulated or downregulated in the DEG comparison SNI vs. sham groups for males and females after removing Rpl and Rps genes. If there were less than 40 genes in any condition, fewer were considered for the analysis. For the analysis of pooled clusters 1-6, the 20-top upregulated DEGs from each cluster in each time point for males and females were used. Analysis of cluster 9 in males 3 days post-SNI was done considering the 40-top upregulated DEGs. For the cluster identification, the top-40 upregulated genes were used. An adjusted p-value cut-off of 0.05 was used on each test.

2.1.7 In situ hybridization and imaging

The spatial and temporal distribution of microglia within the spinal cord was determined using *in situ* hybridization (ISH) with the RNAScope v2 assay. Preliminary scRNA sequencing data from day 3 and day 14 post-SNI/sham surgeries (n=1) was used to

select cluster-specific markers for RNAScope probes, listed in Appendix Table A1. Mice were anesthetized and perfused transcardially with PBS followed by freshly made 4% paraformaldehyde (PFA). Spinal cords were removed from SNI/sham mice 3- and 14-days post-surgery and fixed for additional 24 hrs in 4% PFA at 4°C. Spinal cords were placed overnight in 10% sucrose in PBS at 4°C. Then immersed in 20% and 30% sucrose in PBS, each time until the tissue sunk at the bottom of the tube. Afterward, the cords were frozen at -80°C. Before sectioning, the tissue was left to equilibrate at -20°C and embedded in Optimal Cutting Temperature (OCT) media. 14 µm thick sections were cut on the cryostat and mounted on Superfrost Plus Gold Slides (Thermofisher, FT4981GLPLUS). The RNAScope Multiplex Fluorescent V2 Assay (ACD Biosystems, cat#323100) was performed according to the ACD protocol for fixed-frozen tissue. Spinal cord sections were hybridized to a cluster-specific probe and TMEM119 as the microglial marker. Images were acquired on a Zeiss LSM 880 confocal microscope at X20 magnification and processed as maximum intensity projections of confocal z stacks using ImageJ software (v.1.52).

2.1.8 Immunohistochemistry (IHC) and imaging

Mice were anesthetized with isoflurane (1.5%) and perfused transcardially with PBS followed by 4% PFA. Spinal cords were removed 3 days, 14 days and 8 months post-SNI or sham surgery and incubated in 4 % PFA at 4 °C for 24 h before transferring to PBS. Spinal cords were cut into 30 µm thick transverse sections using a Vibratome. Sections were blocked with 10% normal donkey/goat serum in PBS for 1 hour at room temperature. To study APOE expression, the following antibodies were used: rabbit

anti-IBA1(1:500, Wako, 019-19741) and goat anti-APOE (1:100, Millipore Sigma,178479). For proliferation studies rabbit anti-Ki67 (1:500, Abcam, ab15580) and guinea pig anti-IBA1 (1:500, Synaptic systems, 234 004) were used. Primary antibodies were applied overnight at 4 °C diluted in 0.3% Triton X-100 PBS, followed by 3x10 min rinses in PBS at room temperature. Secondary antibodies [Goat anti-rabbit Alexa Fluor 405 (1:500, Thermo Fisher Scientific, A-31556), Donkey anti-goat Alexa Fluor 568 (1:500, Thermo Fisher Scientific, A-11057), Goat anti-guinea pig Alexa Fluor 647 (1:500, Thermo Fisher Scientific, A-21450), Donkey anti-rabbit Alexa Fluor 568 (1:500, Thermo Fisher Scientific. A10042)] were incubated in PBS for 2.5 hours at room temperature and protected from light, followed by 3x10 min rinses in PBS. Finally, tissue was mounted using ProLong Gold Antifade reagent (Thermofisher, P36934). For APOE experiments, confocal stacks were taken at 63X magnification with oil immersion on a Zeiss LSM 880 confocal microscope equipped with an Argon multiline, 405 diode and HeNe 594 and 633 lasers. For Ki67 experiments, images were acquired on a Zeiss ApoTome at 20X magnification. Each group consisted of four mice, with 5 sections of spinal cord dorsal horn ipsi and contralateral to injury being taken from each mouse.

2.1.9 Image analysis and quantification

Images were processed as maximum intensity projections of z stacks using ImageJ software (v.1.52). The analysis of APOE/IBA1 images was done using ImageJ by calculating the Mean Gray Value of respective channels. Ki67/IBA1 images were used for raw counting of the Ki67 signal and IBA1 signal.

2.1.10 Statistical analysis

Data are represented as means \pm SEM. Statistical tests were made on GraphPad Prism software (v7.03) using a one-way ANOVA followed by between-group comparisons using Tukey's post hoc test or unpaired t-test with $p < 0.05$.

2.2 Aim 2

2.2.1 Animals

Tmem119-2A-CreERT2 (C57BL6 background; JAX: 031820) and Ai14 (RCL-tdT; C57BL6 background; JAX: 007914) mice were obtained from the Jackson Laboratory and maintained in house as previously described. Homozygous Ai14 mice were bred to homozygous Tmem119-CreERT2 mice to generate a line with Cre-dependent expression of tdTomato in microglia. For the genotyping of mice, ear tissue was used for DNA extraction with an alkaline buffer (25 mM NaOH, 0.2 mM Na₂EDTA, pH 12) at 100°C for 25 min. The tissue was neutralized with acidic buffer (40 mM Tris-HCl, pH 5). PCR using primers CreERT2-F(GAT CTC CGG TAT TGA AAC TC) and CreERT2-R(GCT AAA CAT GCT TCA TCG TC) was used to confirm the insertion of CreERT2.

2.2.2 Tamoxifen administration

Tamoxifen was administered as described previously.⁽⁸²⁾ Briefly, (Z)-4-Hydroxytamoxifen (4-OHT; Sigma-Aldrich, H7904) was resuspended at 20 mg/ml in ethanol and diluted in sunflower seed oil (Sigma-Aldrich, S5007) at a final concentration of 2 mg/ml in 10% ethanol. Postnatal day (P) 4 transgenic mice received an intraperitoneal injection of 20 μ l of 4-OHT, corresponding to 50 mg/kg body weight, per

day for six consecutive days, for a total dose of 0.25 mg. Otherwise, mice were injected intraperitoneally with tamoxifen (Sigma-Aldrich, T5648) in sunflower seed oil (100 mg/kg body weight, 10 mg/ml stock solution) at 4 weeks of age once per day for five consecutive days.

2.2.3 Neuropathic pain model

Mice were anesthetized with isoflurane (1.5%) and subjected to unilateral SNI or sham surgeries. Surgeries were performed as previously described.(78)

2.2.4 Tissue clearance with X-CLARITY

Spinal cord sections were cleared using the X-Clarity Tissue clearing system (Logos Biosystems). Mice were perfused via transcardial route with PBS followed by 4% PFA. Spinal cords were extracted and post-fixed for 24 hrs in 4% PFA at 4°C. After washing in PBS for 24 hrs at 4°C, samples were incubated for 24 hrs in 15 mL of a hydrogel solution containing 4% X-CLARITY™ Hydrogel Solution (LogosBio, C13103) and 0.25% (wt/vol) X-CLARITY™ Polymerization Initiator (LogosBio, C13104) in PBS at 4°C. Then, the samples were polymerized at -90 kPa, 37°C for 3 h. The tissue was transferred to the single-chamber and placed in the clearing system. The Electrophoretic Tissue Clearing Solution (LogosBio, C13001) was circulated through the chamber with the following conditions: 37°C temperature, 1.2 A current, 30 r.p.m. pump speed. The clarification process lasted 2 days for a 6-mm-long section of the spinal cord. Once cleared, the samples were kept in PBS at room temperature (RT).

2.2.5 3D image acquisition

Before imaging, the samples were immersed in the RI-matching solution, EasyIndex (Lifecanvas technologies) overnight at RT. Fluorescence imaging of X-CLARITY samples was performed using a light-sheet fluorescence microscope (Carl Zeiss LSM Z.1, Zena, Germany) with a detection objective W Plan-Apochromat 20X/1.0 and illumination objective LSM 10X/0.2. EasyIndex solution was used to match the RI. The plane was illuminated from the right side.

2.2.6 Image processing and quantification

Stacks were processed using Imaris software. First, .czi files were converted into .ims files using Imaris File Converter (v.9.7.0). Then, images were reconstructed in 3D using Imaris Stitcher (v.9.7.2). Reconstructed images were resampled to reduce the file size. The XY ratio was maintained, and the original x-value was divided by three. For the quantification of microglia, the spinal cord was divided in four regions of interest (ROIs) using the Surface tool from Imaris (v.9.7.2). ROIs corresponded to the dorsal and ventral horns, ipsi and contralateral to the injury. ROIs were defined by drawing contours with a 30 μm vertex spacing in stacks on the XY plane every 200 μm . Then, microglia were quantified within each ROI using the Spots tool, with an estimated XY diameter of 10 μm and setting a specific quality filter in each sample. Spots were divided according to their position along the spinal cord (rostral-caudal) every 250 μm .

3. Results

3.1 Transcriptional landscape of spinal microglia at the single cell level after peripheral nerve injury

We performed single-cell RNA sequencing to characterize the transcriptional states of microglia in the development and maintenance of neuropathic pain. Mice were subjected to the spared nerve injury (SNI) model of neuropathic pain. SNI is a robust assay of peripheral nerve injury-induced neuropathic pain, with mechanical hypersensitivity that persists for months in male and female mice. We collected and sequenced single microglia from the lumbar spinal cord of male and female mice at day 3, day 14, and 5 months post-SNI and their age-matching sham controls. The three time points correspond to an early pain development phase, a sub-chronic phase, and a chronic phase, respectively. We processed naïve male and female mice as well. We sampled two replicates per condition, consisting of four mice pooled per replicate. Microglia from the lumbar spinal cord of naïve, sham, and SNI mice were FACS sorted, gating for CD45^{low}CD11B^{high}CX3CR1^{high} cells, and sequenced using the 10X Genomics Chromium platform. Unsupervised clustering analysis of pooled single-cell RNA sequencing data from SNI, sham, and naïve samples revealed eleven distinct microglia clusters (Fig. 1A). In total, 112 mice and 188,787 cells were included in the study. Clusters 1 to 6 aggregate together in the UMAP and account for most of the cells, with approx. 98% of cells in naïve mice (Fig. 1B). All the clusters highly express canonical microglial genes, including *Fcrls*, *Cx3cr1*, *P2ry12*, *C1qa*, *Trem2*, and *Tmem119* (Fig. 2). Gene expression analysis allowed the identification of uniquely expressed genes in

seven of the clusters (Fig. 3), as well as the genes with the highest expression level in each microglia cluster, with the top 5 listed in Table 1.

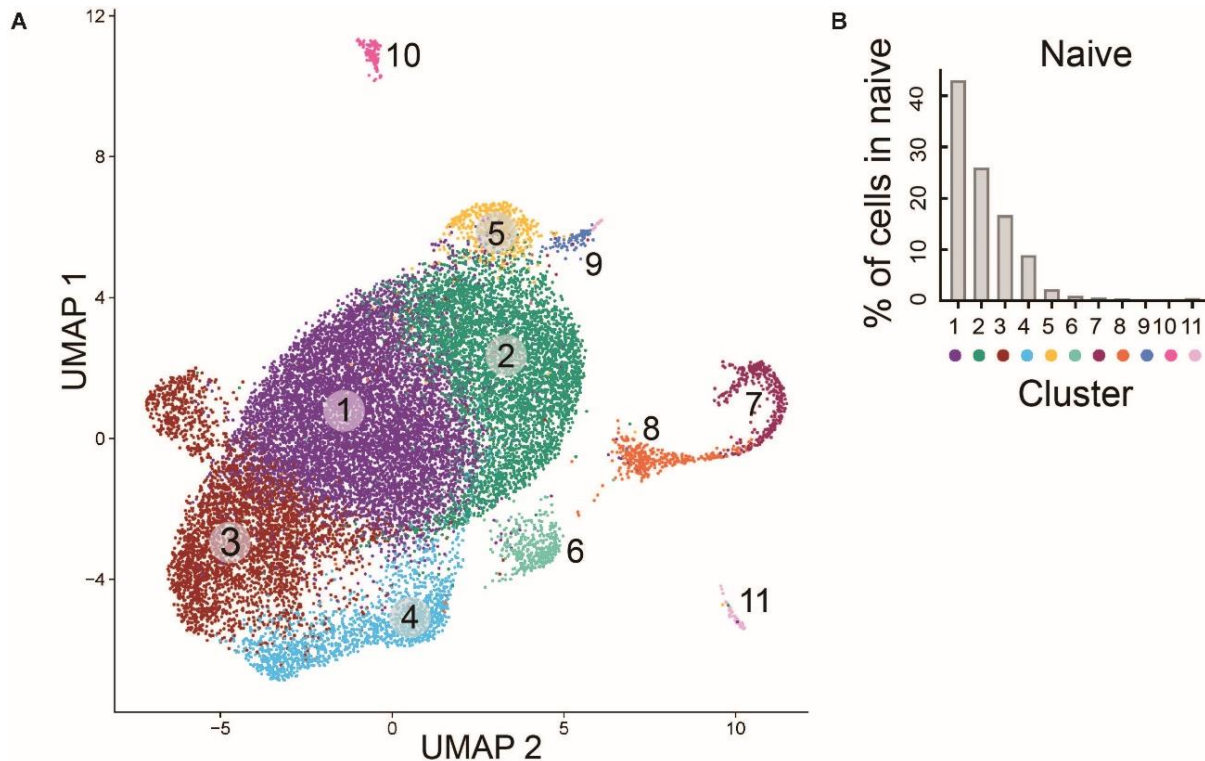


Figure 1. Characterization of microglia at the single-cell level after nerve injury. A) UMAP plot of all single cell included in the study (n= 188,787 cells). In total, eleven clusters were identified. n=112 mice. **B)** Proportion of microglia cells belonging to each cluster in naive mice.

To define the cluster identity, we performed gene ontology (GO) enrichment analysis.

Pooling of top cluster markers from clusters 1 to 6 revealed enriched cytokine-mediated signaling pathways and cellular response to type I interferon processes (Fig. 4).

Clusters 7 and 8 showed enriched DNA replication and cell cycle processes. More specifically, cluster 8 is involved in G1/S cell cycle phases and cluster 7 with G2/M phases. This suggests that cells in clusters 7 and 8 correspond to proliferating microglia. Cluster 9 analysis indicated mitochondrial ATP synthesis and cytokine-

mediated signaling pathway, among other processes. Cells in cluster 10 express the mentioned microglial canonical genes, along with *Cldn5* as the top marker gene of the cluster. *Cldn5* encodes for Claudin-5, a tight-junction protein expressed in endothelial cells but also vessel-associated microglia.(83) Lastly, cluster 11 showed high expression of macrophage and monocyte markers (*H2-Aa*, *Mrc1*, *Ccr2*, *Lyve1*, *Dab2*, *Mgl2*, *F13a1*), which indicates that these cells might be perivascular and meningeal macrophages that express both macrophage and microglial genes.

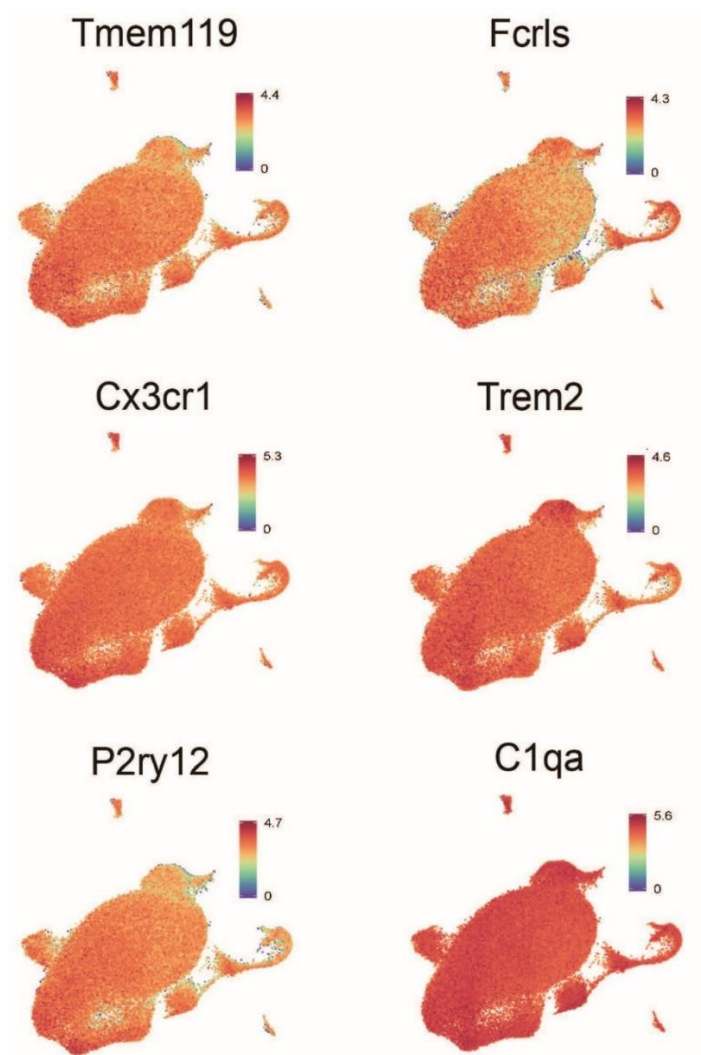


Figure 2. UMAP plot colored for the expression (log-normalized counts) of canonical microglial genes.

Table 1. Top five upregulated genes per cluster.

Cluster	1	2	3	4	5	6	7	8	9	10	11
	<i>Nr4a1</i>	<i>Gpr84</i>	<i>Rgs1</i>	<i>Gm3336</i>	<i>ApoE</i>	<i>Ifit3</i>	<i>Mki67</i>	<i>Stmn1</i>	<i>Ifi2712a</i>	<i>Cldn5</i>	<i>H2-Eb1</i>
	<i>Ddit3</i>	<i>Cd14</i>	<i>Txnip</i>	<i>Gm26802</i>	<i>spp1</i>	<i>Ifitm3</i>	<i>Top2a</i>	<i>Cxcl10</i>	<i>Tspo</i>	<i>Ly6c1</i>	<i>H2-Aa</i>
	<i>Ccr12</i>	<i>Il1b</i>	<i>Tmx4</i>	<i>Rsrp1</i>	<i>Plp</i>	<i>Ccl12</i>	<i>Stmn1</i>	<i>Tubb5</i>	<i>Ly86</i>	<i>Itm2a</i>	<i>H2-Ab1</i>
	<i>Gem</i>	<i>Il1a</i>	<i>Rhoh</i>	<i>Fbxl18</i>	<i>Lyz2</i>	<i>Isg15</i>	<i>Cenpf</i>	<i>Mcm3</i>	<i>Rps2</i>	<i>Flt1</i>	<i>Lyz2</i>
	<i>Atf3</i>	<i>Pim1</i>	<i>Gpr183</i>	<i>Milr1</i>	<i>Cd63</i>	<i>Ifi204</i>	<i>Cxcl10</i>	<i>Lig1</i>	<i>Rpsa</i>	<i>Spock2</i>	<i>ApoE</i>

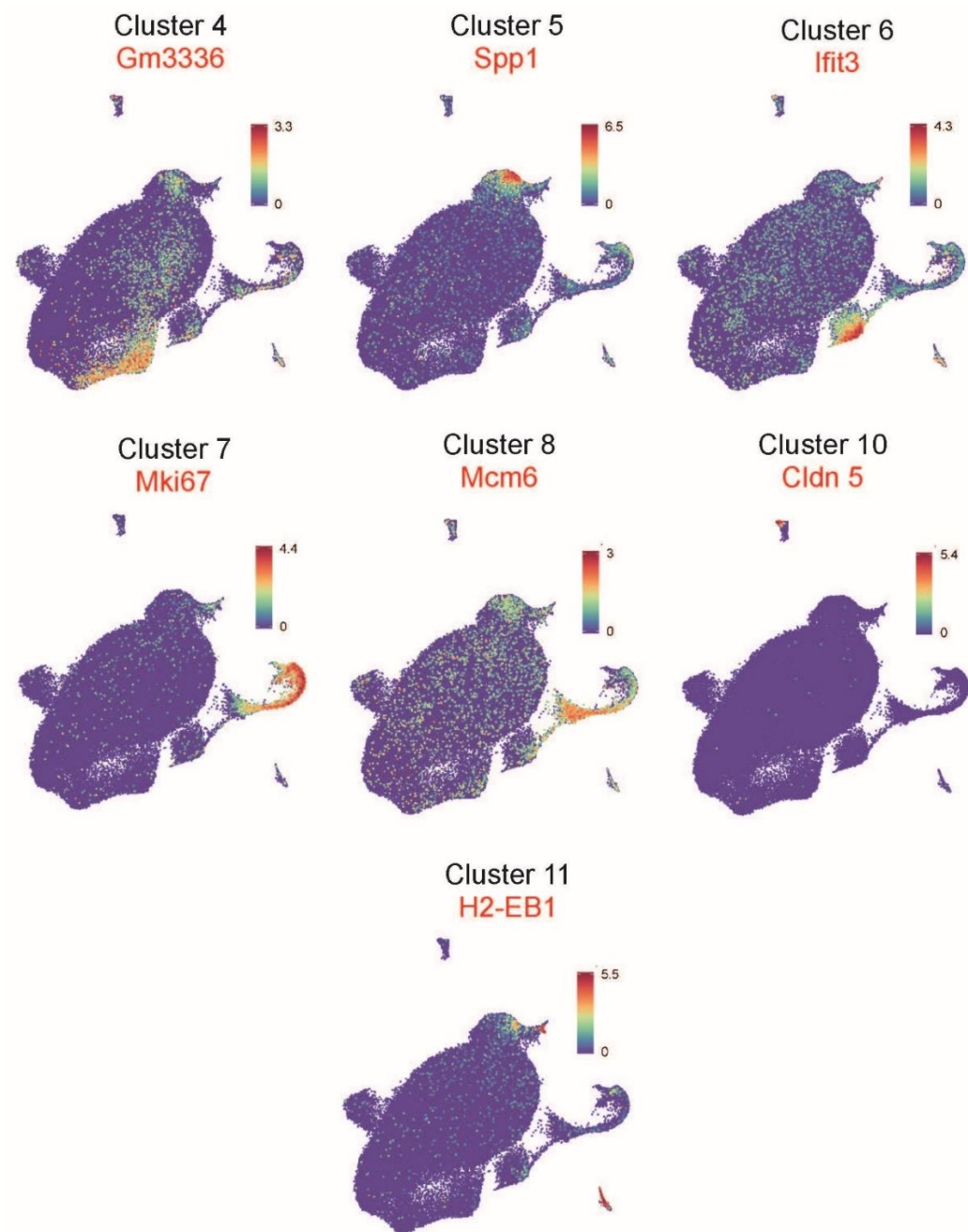


Figure 3. UMAP plot colored for the expression (log-normalized counts) of the top unique gene in the indicated microglial cluster. Genes uniquely expressed in 7 of the 11 clusters were found.

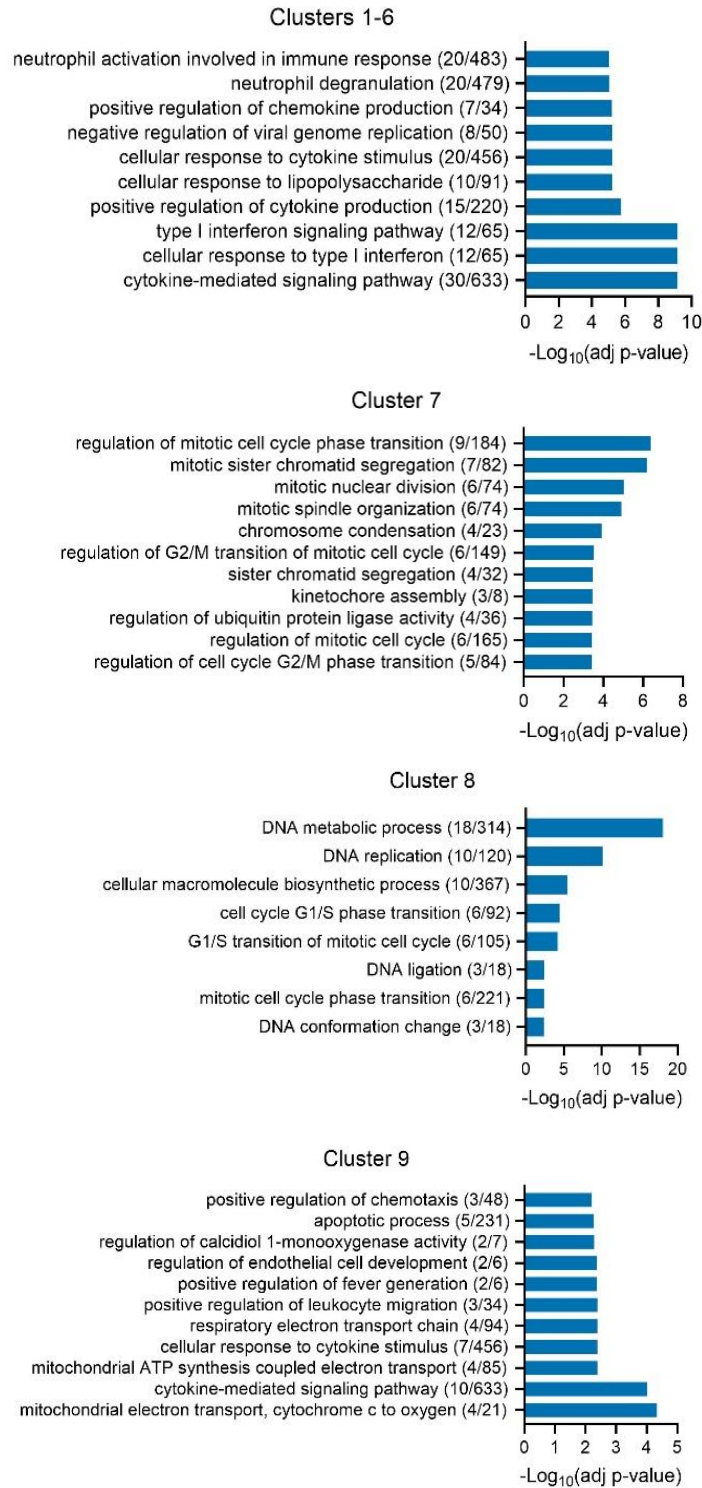


Figure 4. Gene Ontology terms (biological process) enriched in markers from clusters 1-6, 7, 8 and 9. The 40-top upregulated DEGs from each cluster were used for the analysis after removal of ribosomal proteins.

3.2 Sex-specific changes in the transcriptome of microglia after peripheral nerve injury

Comparative analysis of the transcriptome of naïve male and female mice revealed 179 distinct DEGs, of which 138 were upregulated in males and 42 upregulated in females. Several genes were upregulated in more than one cluster. GO analysis of these DEGs revealed that naïve female mice have enriched processes related to cholesterol transport when compared to male mice, whereas males display enrichment for genes involved in mRNA translation (Fig. 5).

To study how peripheral nerve injury alters transcriptional states in microglia, we determined differentially expressed genes (DEGs) in SNI versus sham groups in each microglia cluster at three-time points in male and female mice (Fig. 6A-B). On day 3 post-SNI, males and females displayed the highest number of DEGs. However, males showed more DEGs than females at all time points. In addition, only a fraction of the DEGs from males and females was shared. On day 3, only 92 DEGs were shared out of 475 DEGs in males and 260 in females. On day 14, there were 22 common DEGs (130 in males, 77 in females), and at 5 months post-SNI only 18 DEGs were in both lists (140 DEGs in males, 116 in females). We found that several ribosomal protein genes (small ribosomal subunit (*Rps*) and large ribosomal subunit (*Rpl*)) showed significant changes in the transcription levels in male mice, with upregulated *Rpl* and *Rps* genes at day 3 and 14 and downregulated at 5 months post-SNI (Fig. 6C).

Interestingly, we found some sex differences in the expression of inflammation-related genes. The MAPK-specific phosphatases *Dusp1* and *Dusp6* were down-regulated exclusively in males in clusters 3, 8, and 9 at day 3 post-SNI but not at later time points

(at day 14 or 5 months); conversely, *Dusp6* was upregulated in female microglia in five clusters (Table 2). The pro-inflammatory genes *Il1b* and *Tnf* were specifically upregulated in males at day 3 post-SNI. *Tspo*, a microglia activation marker, was found to be upregulated in both sexes (Table 2).

To gain insight into the processes occurring in female and male microglia from the spinal cord following peripheral nerve injury, we performed gene ontology (GO) enrichment analysis on DEGs (after removal of ribosomal protein genes) in each cluster and pooling of top 20 DEGs from clusters 1 to 6 in males and females (Fig. 7). Nerve injury induces a strong immune response at day 3 in males (top GO terms: cellular response to cytokine stimulus, cytokine-mediated signaling pathway, inflammatory response), whereas females display a weaker inflammatory response with top GO terms such as ATF-6-mediated unfolded protein response and receptor-mediated endocytosis (Fig. 7). On day 14, males have as top GO terms mitochondrial ATP production and other metabolic processes, including cholesterol efflux. At this time point, females have enriched endocytosis/phagocytosis, cell adhesion, and lipid catabolism processes. Lastly, at 5 months post-SNI, microglia in males show changes in the mitogen-activated protein kinase (MAPK) signaling, while microglia in females exhibits changes in metabolic processes and responses to lipopolysaccharide.

As previously mentioned, clusters 1 to 6 account for most of the sequenced cells, with approx. 98% of cells in naïve mice. Nevertheless, we found some differences between male and female mice in the proportion of microglia from clusters 7, 8, and 9 (Fig. 8). Microglia belonging to cluster 9 were absent in naïve mice (0.035%) but their presence was considerably increased 3 days post-SNI in males (4.9%) but not in females (0.03%)

(Fig. 9A). By day 14, microglia from cluster 9 were basically undetected in both sexes. Microglia from the male-specific cluster 9 showed enriched processes related to acute inflammatory response and mitochondrial ATP production (Fig. 9B). Additionally, cluster 9 in males at day 3 post-SNI displayed a transcriptional profile highly similar to the injury-responsive microglia (IRM) (Fig. 9C, Fisher's exact test: $p=5.8 \times 10^{-68}$). The IRM signature was found after lysolecithin (LPC)-induced demyelination, a common model of multiple sclerosis.(55)

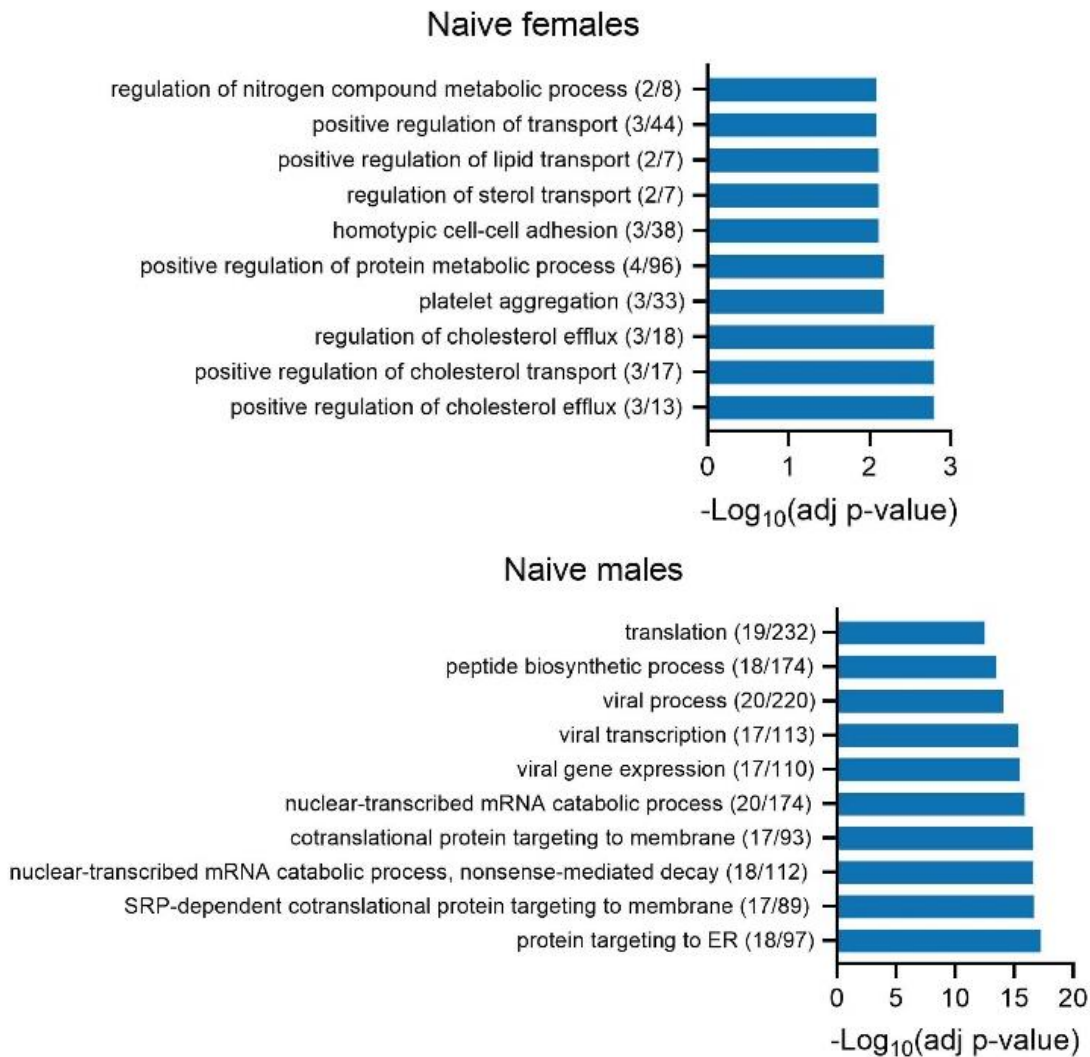


Figure 5. GO analysis of microglia from naïve female and male mice. GO terms (biological process) of differentially expressed genes (DEGs) upregulated in female or male naïve mice.

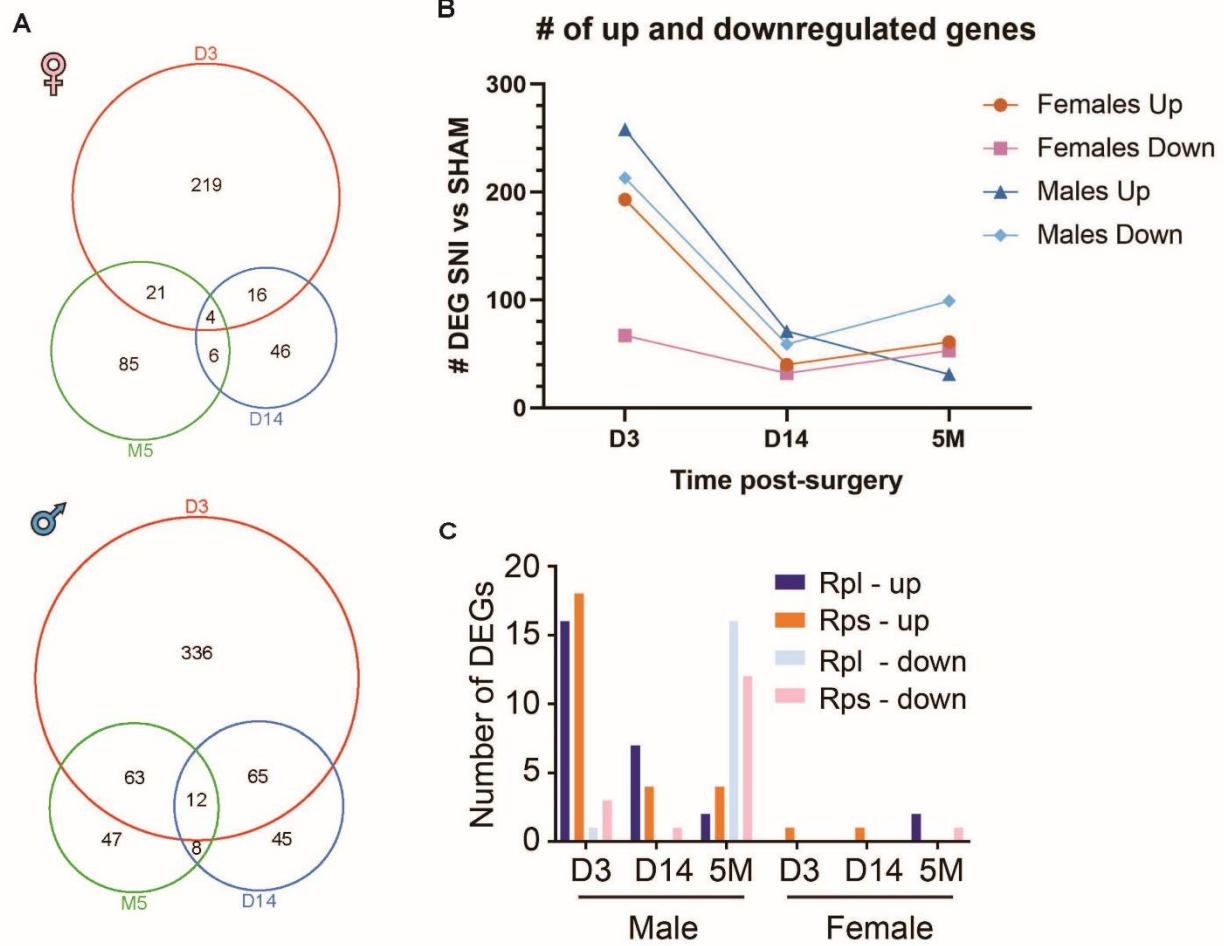


Figure 6. Sex-specific changes in the transcriptome of microglia after peripheral nerve injury. A) Number of DEGs from the comparison of SNI and sham samples at day 3, day 14 and 5 months in females (top) and males (bottom). **B)** Number of upregulated and downregulated DEGs in each sex and time point. **C)** Number of upregulated and downregulated genes encoding for large (Rpl) and small (Rps) ribosomal protein subunits.

Table 2. Fold change of MAPK and inflammation related genes. Upregulated genes are shown in red and downregulated in blue. Adjusted p-values are shown in brackets. The p-values were corrected for multiple testing using the Benjamini-Hochberg method.

Time point		Day 3		Day 14		Month 5	
Gene	Cluster	Males	Females	Males	Females	Males	Females
<i>Dusp1</i>	2			0.266 (3.16E-55)			
	3	-0.342 (1.069E-28)					
	5			0.368 (3.52E-10)			
	6			0.296 (0.007)			-0.269 (4.95E-03)
	9	-0.523 (0.015)					
<i>Dusp2</i>	1		-0.500(3.41E-42)				
	2				0.342(4.33E-18)		
	3	0.532(6.72E-22)	-0.316(1.78E-04)				
	6		-0.849(0.001624)				
	8	0.293(3.84E-02)					
<i>Dusp6</i>	1		0.490 (4.26E-93)				
	2		0.390 (2.04E-33)				
	3	-0.428 (1.07E-26)	0.354 (7.73E-21)				
	4		0.261 (5.16E-03)				
	7		0.341 (0.010)				
	8	-0.386 (1.141E-04)					
<i>Il1b</i>	1	0.861 (1.40E-59)	0.311 (5.46E-16)		0.280 (7.10E-14)		
	2	0.504 (1.57E-12)			0.282 (2.84E-03)		
	3	0.531 (3.74E-07)	0.449 (2.86E-04)				
	7	0.926 (1.61E-11)					
	8	0.847 (3.21E-06)					
	9	1.70 (3.78E-05)					
<i>TNF</i>	1	0.471 (4.02E-77)					
	2	0.280 (3.87E-09)			0.292 (2.81E-20)		
	3	0.711 (6.77E-47)					
	6	0.552 (0.008)					
	7	0.537 (5.29E-15)					
	8	0.570 (1.63E-14)					
	9	0.879 (5.67E-08)					
<i>Tspo</i>	1	0.375 (1.29E-69)	0.295 (2.59E-47)				
	2		0.267 (1.02E-23)				
	3	0.419 (1.13E-30)	0.366 (4.63E-21)				
	4	0.376 (3.56E-09)	0.319 (5.16E-05)				
	5	0.366 (0.015)	0.405 (0.001)				
	6			0.486 (2.96E-06)			
	8	0.286 (1.07E-07)		0.698 (0.029)			
	9	0.639 (2.32E-06)					
<i>Nfkbia</i>	1		-0.252 (1.39E-65)				
	2			0.364 (5.95E-110)			
	3		-0.262 (2.36E-14)			0.250 (2.72E-34)	
	4			0.282 (4.22E-09)			
<i>Abca1</i>	4			0.300 (3.64E-11)			
<i>Npc2</i>	6			0.296 (2.96E-06)			

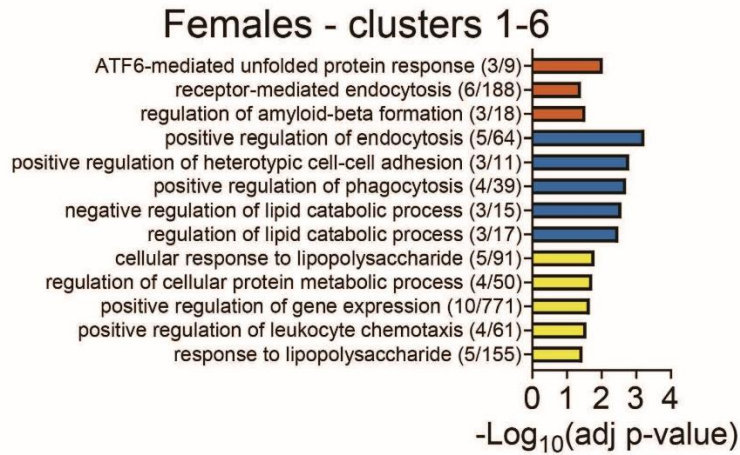
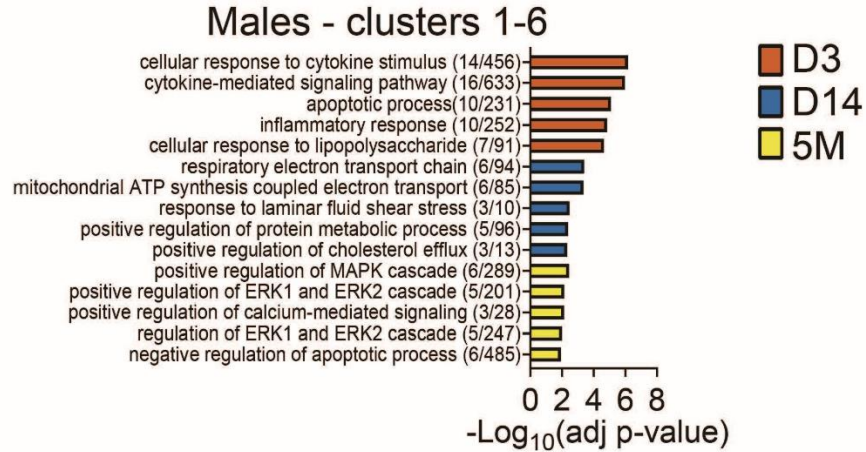


Figure 7. GO analysis of males and females after peripheral nerve injury. GO terms (biological process) of DEGs in males and females in each time point for clusters 1-6. The 20-top upregulated DEGs from each cluster were used for the analysis after removal of ribosomal proteins.

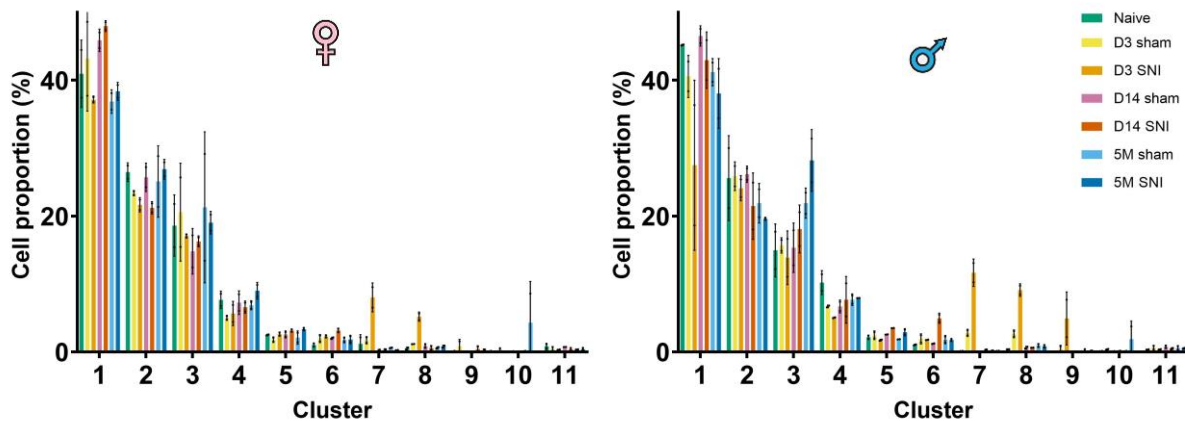


Figure 8. The cell proportion varies across the different microglia clusters. Plot of the percent of cells per condition in females (right) and males (left) that were assigned to each cluster. Data are expressed as mean \pm SEM.

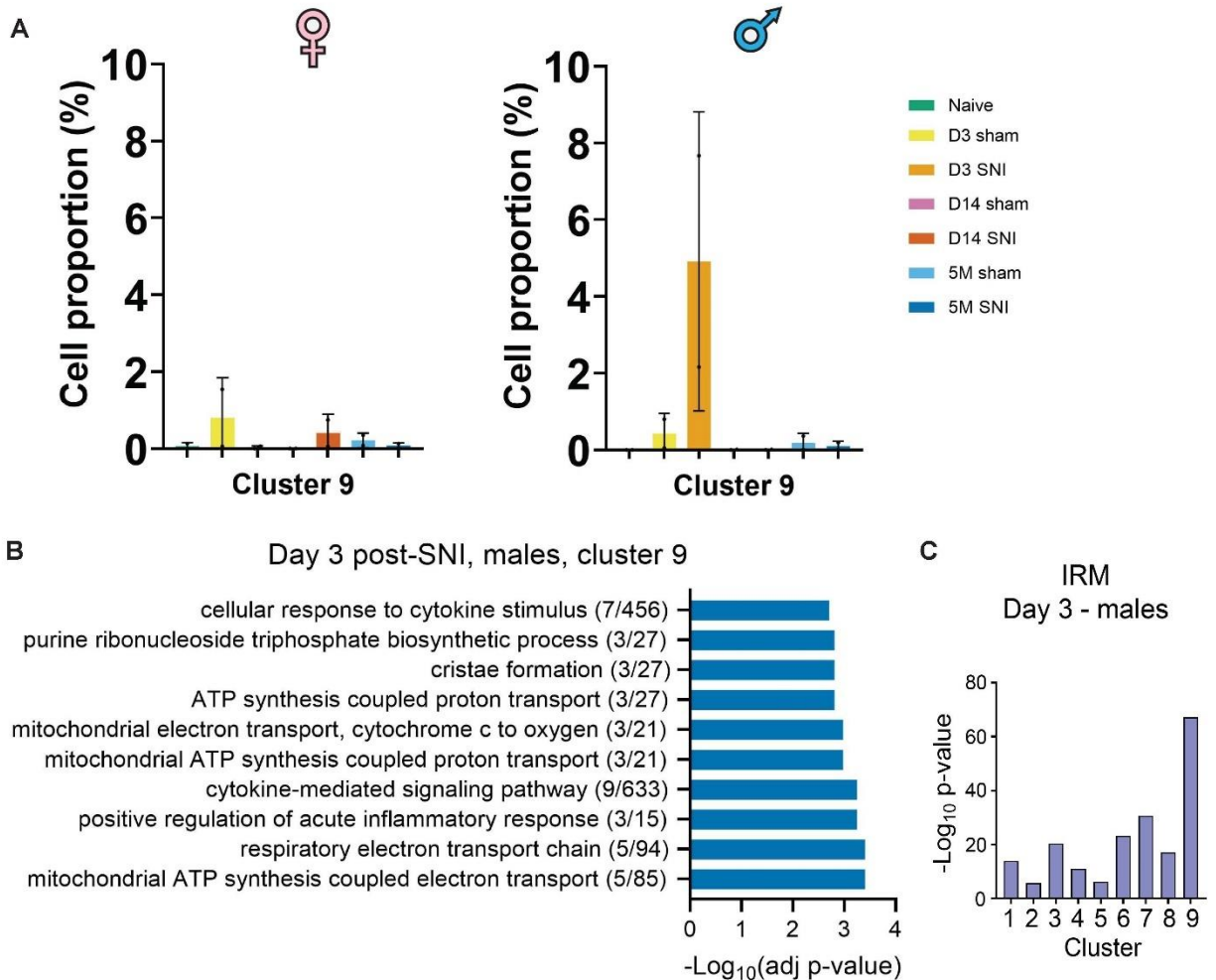


Figure 9. Peripheral nerve injury gives rise to a male-specific cluster of microglia. A) Proportions of cells in cluster 9 in females (left) and males (right). **B)** GO terms (biological process) of cluster 9 at day 3 post-SNI in males. The 40 top upregulated genes were used for the analysis. **C)** Enrichment for IRM signature in males in clusters 1 to 9 at day 3 post-SNI (Fisher's exact test).

3.3 Peripheral nerve injury induces greater proliferation of microglia in the lumbar spinal cord of male mice as compared to female mice

As mentioned above, microglia in clusters 7 and 8 highly express the cell cycle-associated markers *Mki67* and *Top2a* (Table 1) and show enriched DNA replication and cell cycle processes (Fig. 2). Plotting cell proportion of microglia across time points and conditions revealed an increase in these proliferating microglia on day 3 post-SNI (Fig.

10). Surprisingly, the increase was larger in male mice as compared to female mice. In males, the percentage of microglia from clusters 7 and 8 increased from 0.5% in naïve mice to 5.4% in sham and 20.8% in SNI mice; while in females, the proportion increased from 1.7% in naïve mice to 2.9% in sham and only 13.2% on day 3 post-SNI (Fig. 10A-B). Using sequencing data, we defined unique cluster markers and performed ISH (RNAscope). *Cdca3* was selected as the marker for the proliferating cluster, and *Tmem119* was used to label microglia. The proliferating cluster was prominently present in the superficial laminae and the ventral horn. RNAscope data also showed a reduction in proliferating cells in female mice 14 days post-SNI, similarly to findings from the transcriptomic data (Fig. A1).

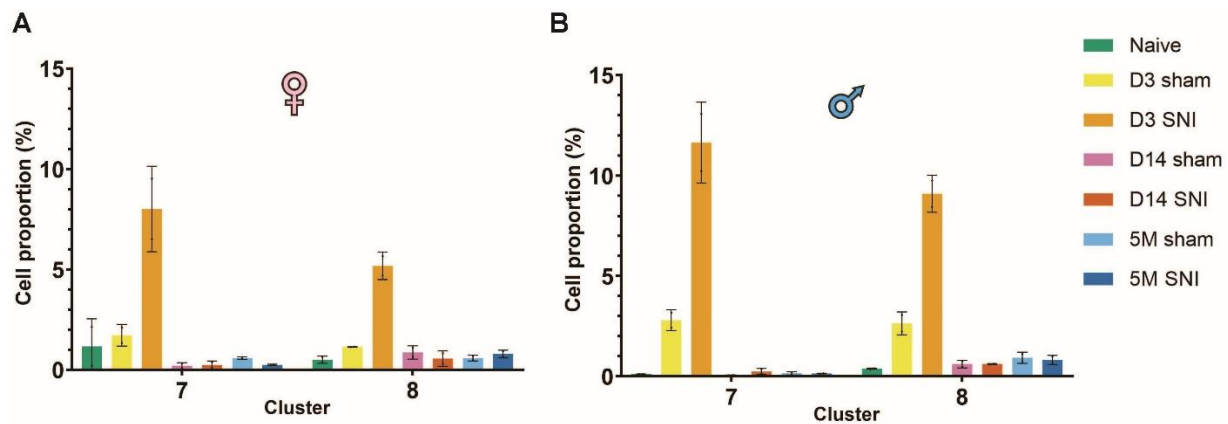
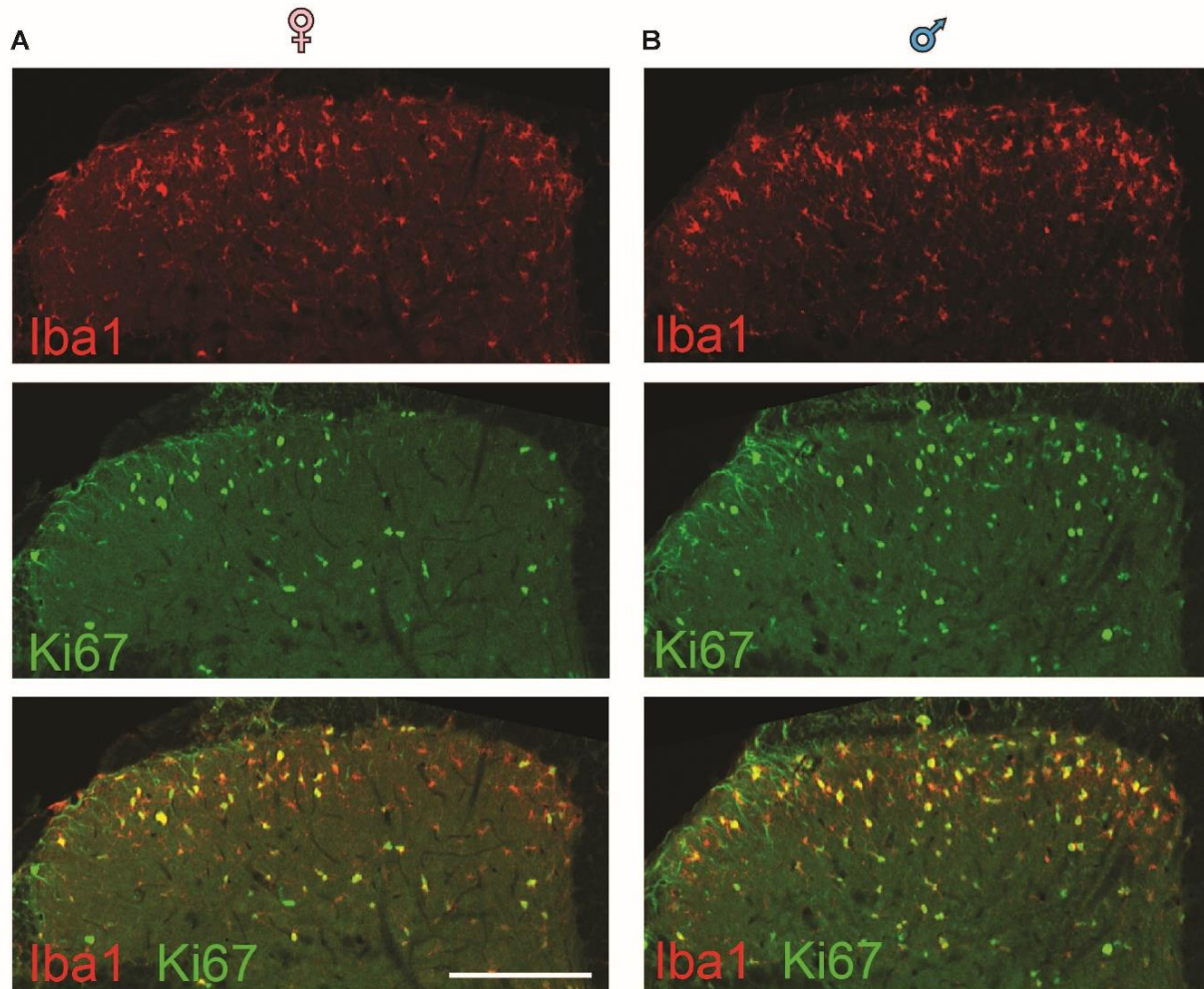


Figure 10. Peripheral nerve injury changes the proportion of microglia belonging to the proliferating clusters. Proportion of microglia in clusters 7 and 8 in females (A) and males (B). Data are expressed as mean \pm SEM.

To confirm that microglia in male mice proliferate more than microglia in females after peripheral nerve injury, we co-stained with Ki67, a proliferation marker, and IBA1, a microglial marker. The quantification of Ki67⁺ microglia in the dorsal horn spinal cord of wild type mice (Fig. 11A-C) showed that the number of proliferating microglia was

significantly higher in males as compared to females (Ki67⁺ microglia per section; males: 68.8 ± 5.9 ; females: 46.6 ± 1.8 , $p=0.011$, Fig. 5C), confirming the transcriptomics result. However, the total number of IBA1⁺ microglia was not different between male and female mice (IBA1⁺ microglia per section, males: 82.8 ± 5.5 ; females: 76.4 ± 1.8 , $p=0.31$, Fig. 11D), which suggests differences in the mechanism underlying microgliosis between males and females after peripheral nerve injury. Since IBA1 can also label infiltrating macrophages, we repeated this experiment using *Tmem119*^{CreERT2}; Ai14 mice which express tdTomato under the promoter of *Tmem119*, a specific microglia marker. We replicated our finding with the IBA1 staining and found a higher number of Ki67⁺ microglia in the dorsal horn spinal cord of males as compared to females ($p=0.001$, Fig. 12A-C) and similar levels of microgliosis between males and females ($p=0.381$, Fig. 12D).



C57BL/6J

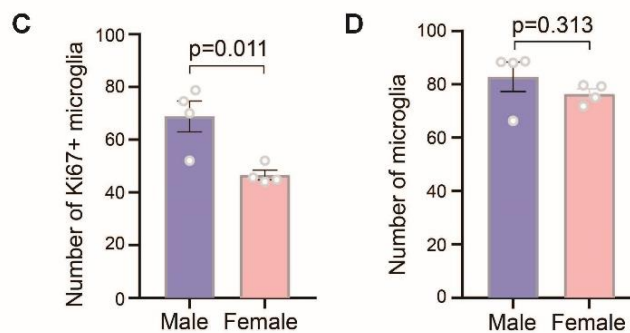
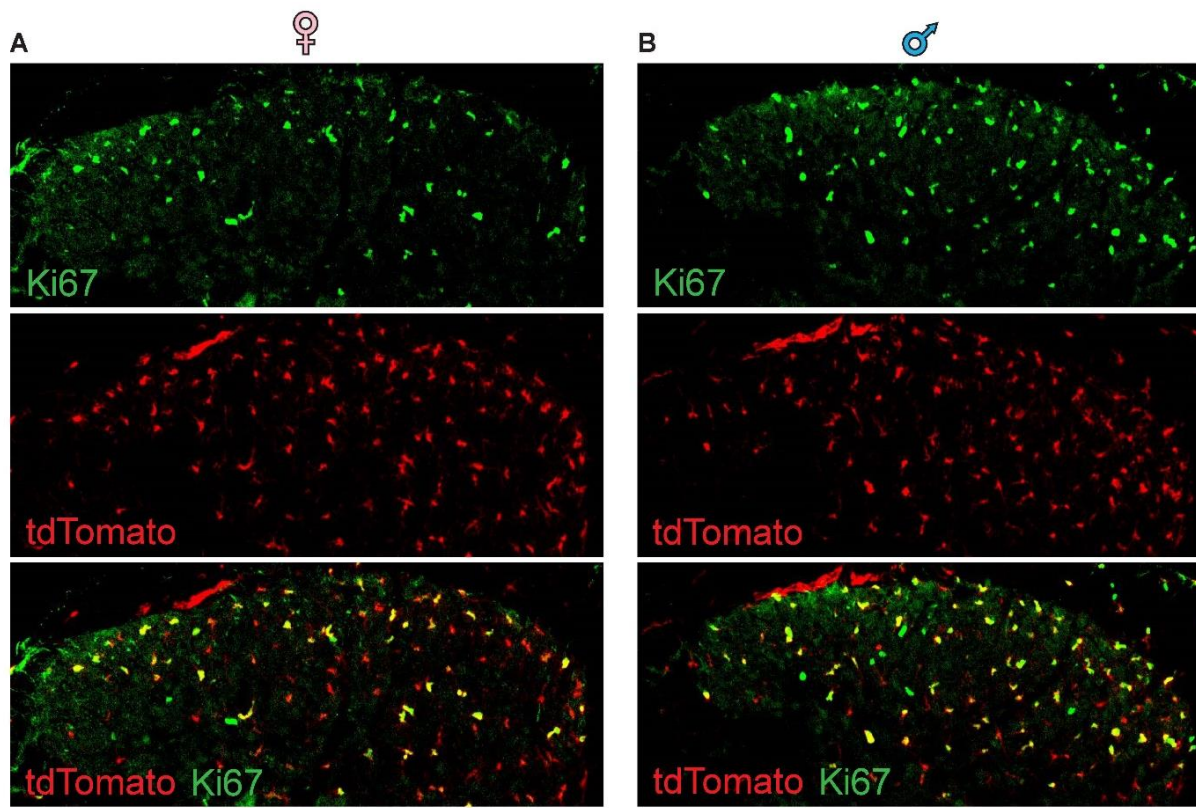


Figure 11. Peripheral nerve injury induces greater proliferation of microglia in males as compared to females. IBA1 (microglia, red) and Ki67 (proliferating cells, green) immunostaining shows proliferating microglia at day 3 post-SNI in female (A) and male (B) wild-type C57BL/6J mice. C) Quantification of proliferating microglia and D) the total number of microglia in wild-type mice (n=4 mice/group). An unpaired t-test was used to compare the two groups. Data are plotted as mean ± s.e.m.



Tmem119CreERT2;Ai14

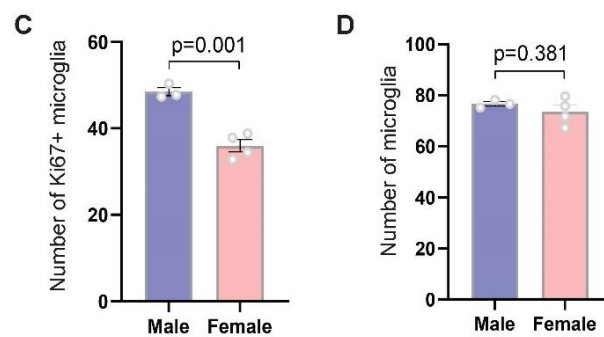


Figure 12. Peripheral nerve injury induces greater proliferation of microglia in males as compared to female Tmem119CreERT2; Ai14 mice. tdTomato (microglia, red) and Ki67 (proliferating cells, green) immunostaining shows proliferating microglia at day 3 post-SNI in female (A) and male (B) Tmem119CreERT2; Ai14 mice. **C)** Quantification of proliferating microglia and **D)** the total number of microglia in Tmem119CreERT2; Ai14 mice (n=3 or 4 mice/group). An unpaired t-test was used to compare the two groups. Data are plotted as mean \pm s.e.m.

Given that males display enhanced proliferation, we hypothesized that microglial cells in males undergo apoptosis at higher rates than females, compensating for increased proliferation while maintaining similar levels of microgliosis. To test this hypothesis, we performed immunostaining against cleaved caspase-3 (CC3), which labels apoptotic cells, and IBA1, a microglial marker (Fig. 13A-B). We did not find apoptotic microglia in male mice on day 3 post-SNI (Fig. 13C). This agrees with previous findings where apoptotic cells were found in rats 7 days after SNI.(84)

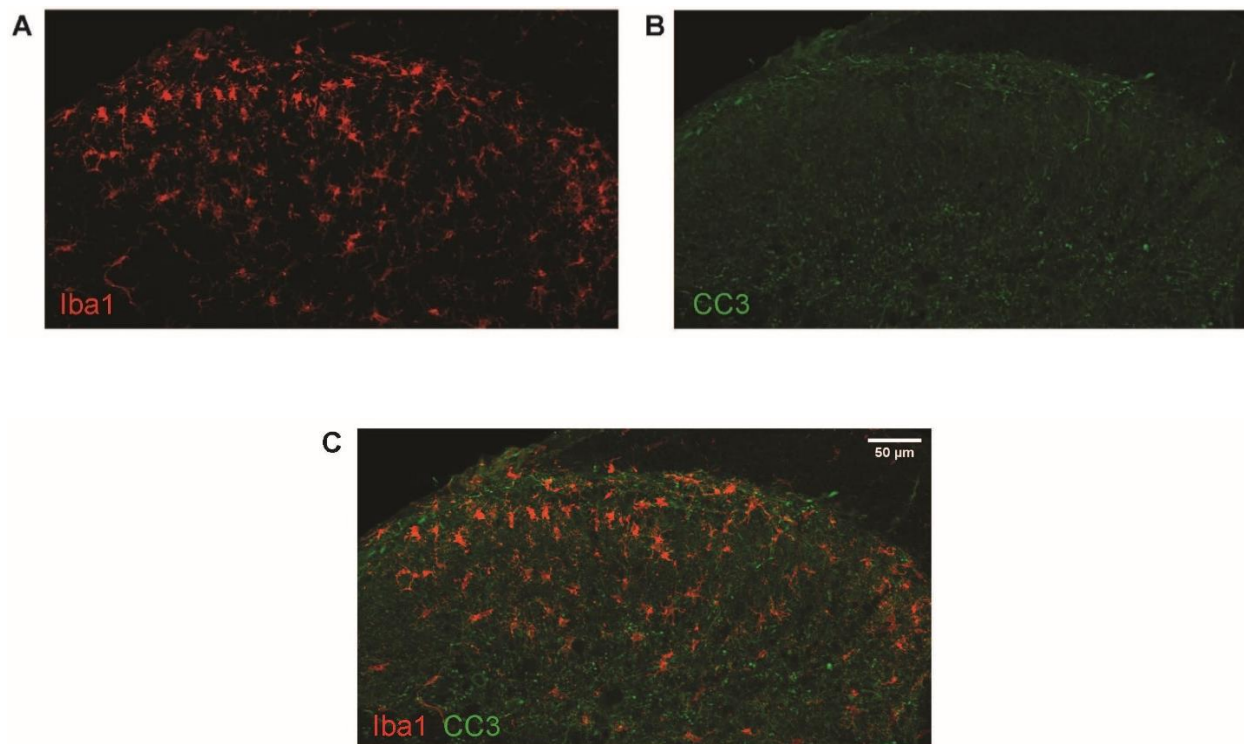


Figure 13. Cleaved caspase-3 immunoreactivity in the spinal cord of a male mouse 3 days post-SNI. A) IBA1 (microglia, red) and **B)** CC3 (apoptotic cells, green) immunostaining. The merging of these images in **C)** shows that microglia are not CC3 positive 3 days post-SNI.

3.4 Apoe is upregulated in spinal microglia at chronic phases of neuropathic pain

Apolipoprotein E (APOE) is a protein involved in lipid metabolism and trafficking and has been linked to different neurodegenerative diseases.⁽⁸⁵⁾ *Apoe* appeared as the top upregulated gene in spinal microglia from cluster 5 (Table 1, Fig. 14A). Following peripheral nerve injury, *Apoe* mRNA levels showed no expression changes on day 3 post-SNI. However, by day 14 and up to 8 months post-SNI, *Apoe* was significantly upregulated in clusters 1 to 6 in males and females (Table 3), appearing as the top DEG in most clusters. To determine if upregulation of *Apoe* mRNA in microglia leads to changes in APOE protein levels after peripheral nerve injury, we co-stained with APOE and IBA1, a microglial marker (Fig. 15A). APOE levels in microglia were low at day 3 post-SNI but increased significantly at day 14 and 8 months (Fig. 15A-B). These results demonstrate that following SNI, APOE upregulation in microglia persists for several months and suggest that this gene might play a role in microglia's chronic response to peripheral nerve injury.

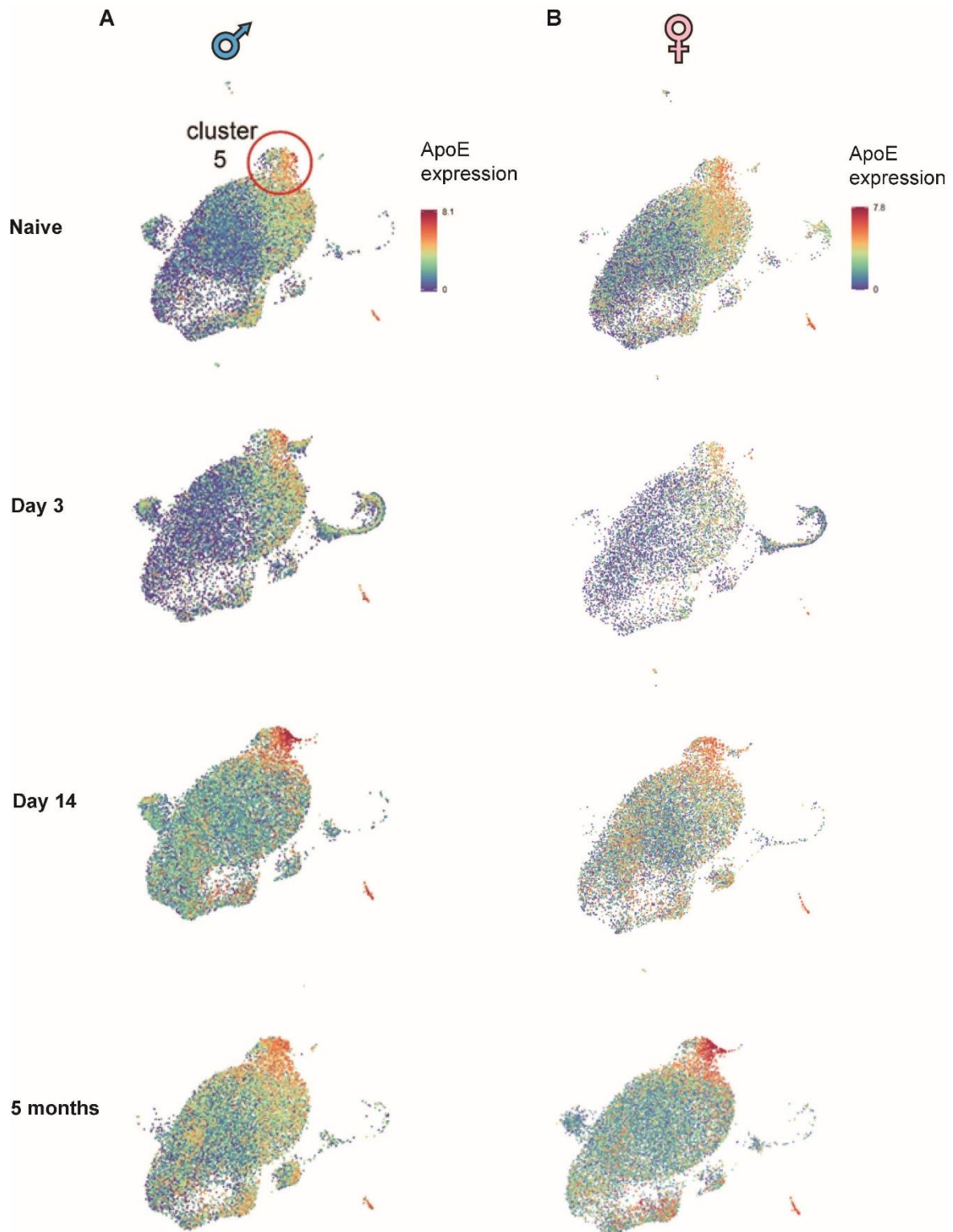


Figure 14. Gene expression of ApoE is increased in microglia in chronic phases of neuropathic pain. UMAPs of ApoE expression (log-normalized counts) in males (A) and females (B) in naïve and SNI mice.

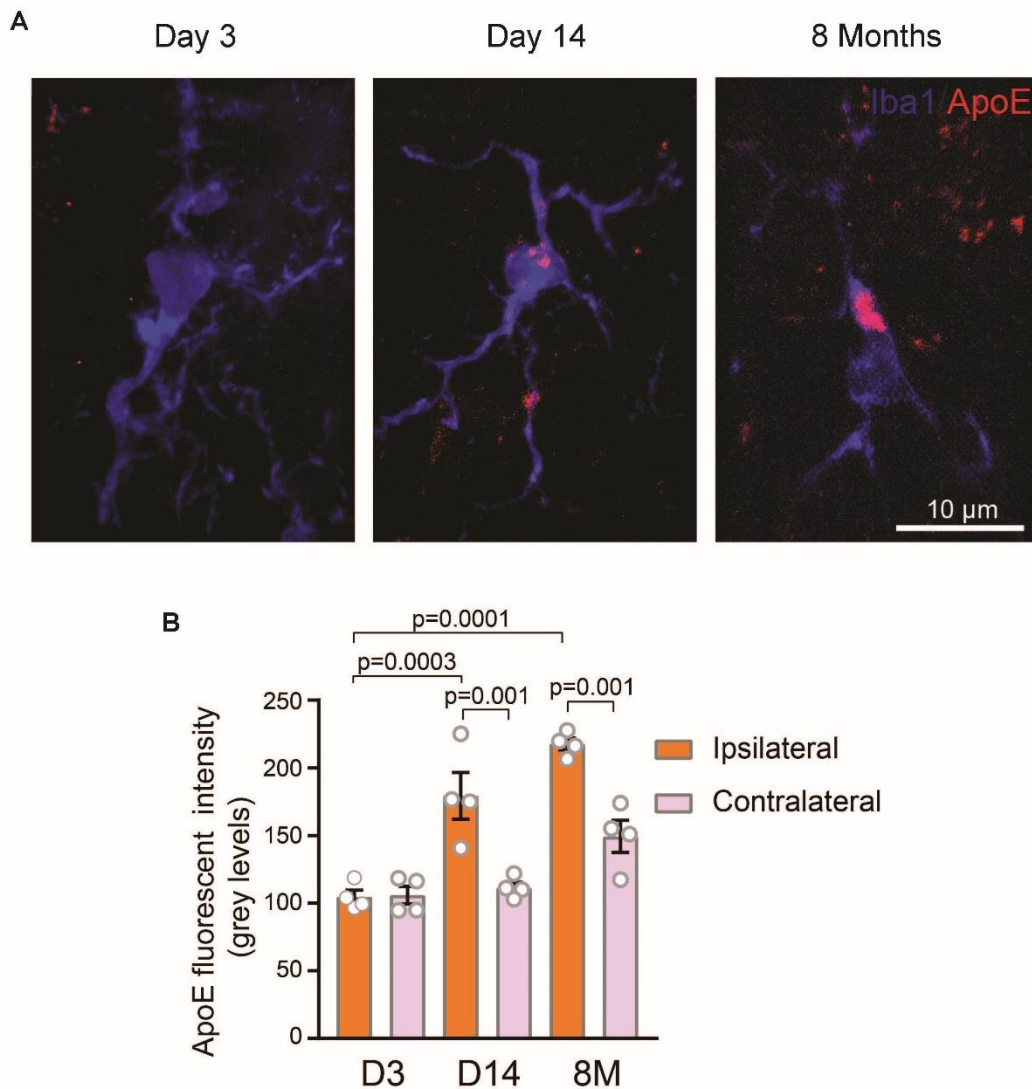


Figure 15. ApoE is increased in microglia in chronic phases of neuropathic pain. A) Representative images of APOE and IBA1 immunostaining in the spinal cord of male mice after SNI. **B)** Quantification of APOE immunostaining signal in microglia (n=4 mice/condition). Ipsi-D3: 104.8 ± 4.9, contra-D3: 106.1 ± 6.5, ipsi-D14: 179.5 ± 17.3, contra-D14: 111.6 ± 3.9, ipsi-8M: 217.5 ± 4.4, contra-8M: 149.5 ± 11.8. Data are plotted as mean ± s.e.m., one-way ANOVA followed by Tukey's multiple comparisons post hoc test.

Table 3. Fold change (LogFC) of *Apoe* mRNA in females and males across time points and clusters.

Time point	Cluster	Females			Males		
		avg logFC	adj p-value	DEG rank	avg logFC	adj p-value	DEG rank
Day 3	1	0.51	4.82E-07	2			
Day 14	1	1.36	1.75E-230	1	1.21	0	1
	2	0.87	6.24E-59	1	0.50	3.75E-52	3
	3	1.26	2.93E-62	1	1.12	1.13E-91	1
	4	0.98	2.36E-17	1	0.85	1.15E-35	2
	5	0.65	0.000602	1			
	6	0.92	0.000106	1	0.29	0.000314	22
Month 5	1	1.01	0	1	1.14	0	1
	2	0.93	1.54E-142	1	1.26	1.21E-127	1
	3	0.75	3.43E-149	1	0.82	8.92E-186	1
	4	1.22	2.69E-56	1	1.47	2.10E-50	1
	5	0.69	6.34E-07	1	1.22	2.55E-29	1
	6	1.14	2.44E-09	1	0.73	4.34E-10	1
	7	1.16	0.000646	1	0.49	0.043917	1
	8						

3.6 LYVE-1 positive cells are observed in the lumbar spinal cord in proximity to blood vessels

3D rendering of cleared spinal cords from *Tmem119^{creERT2/+}; Ai14^{tdTomato/+}* mice revealed differences in the samples where the meninges were kept or removed. tdTomato signal was found in the meninges of intact spinal cord. The expression of TMEM119 has been reported in leptomeningeal cells covering the surface of the brain and lining large blood vessels.(86) Although the meninges harbor the lymphatic system in the brain, lymphatic vessels are absent in the rat spinal cord.(87) However, the lymphatic vessel endothelial hyaluronan receptor 1 (*Lyve1*) gene, a marker for lymphatics vessels, has been shown to be expressed on the surface of the rat spinal cord.(87, 88) Since *Lyve1* appeared as one of the markers for cluster 11, we co-stained for LYVE1, CD31 (endothelial cell

marker) and IBA1 (microglial marker) using horizontal sections of the spinal cord from *Tmem119^{creERT2/+}; Ai14^{tdTomato/+}* mouse. High resolution images allowed us to identify LYVE1⁺ IBA1⁺ tdTomato⁺ cells in proximity to blood vessels (Fig. 16A, F).

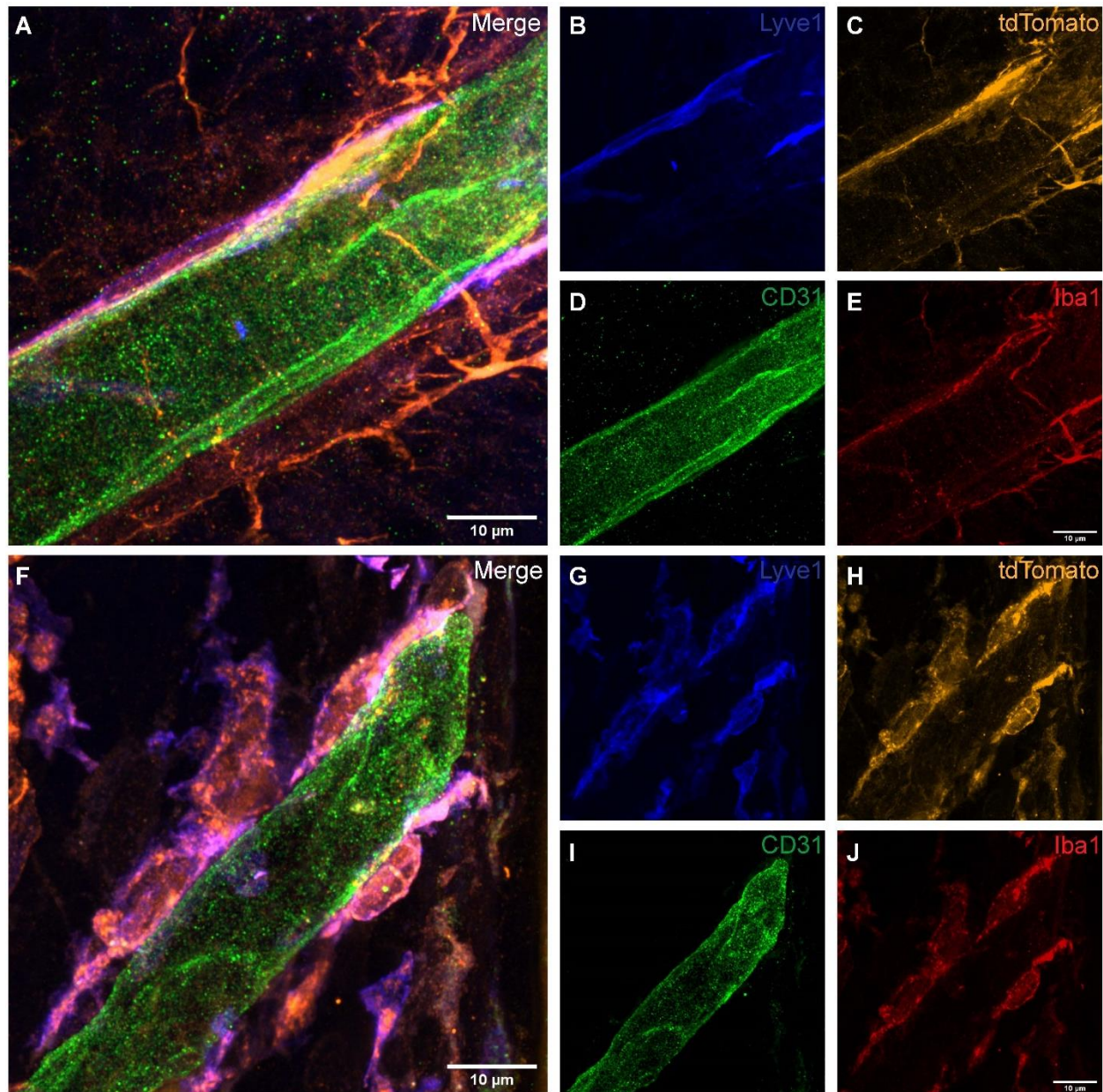


Figure 16. LYVE1 positive cells in proximity to blood vessels in the mouse spinal cord. Horizontal sections of the spinal cord of *Tmem119^{creERT2/+}; Ai14^{tdTomato/+}* mice were stained for **B, G** LYVE-1 (blue), **D** endothelial cell marker CD31 (green) and **E, J** microglial marker IBA1 (red). Microglia was also labeled with **C, H** tdTomato.

3.7 3D imaging of microglia using light-sheet microscopy

To assess whether microgliosis caused by nerve injury differs between male and female mice, we used 3D imaging of fluorescently labeled microglia. *Tmem119-CreERT2* mice were bred to *Ai14* mice to generate Cre-dependent expression of tdTomato in microglia. The spinal cord of *Tmem119-CreERT2: Ai14* mice was cleared with the X-Clarity Tissue clearing system (Fig. 17B). Using light-sheet microscopy, it was possible to generate a 3D reconstruction of the lumbar section of the spinal cord with sufficient resolution to identify and quantify microglia (Fig. 17C, Fig. 18, Fig. 19, Appendix C Fig. C1). We defined the distribution of microglia along the spinal cord in the rostro-caudal axis by using the function Spots from Imaris (v.9.7.2). Three samples of 3 days post-sham mice (1 male, 2 females) and four samples of 3 days post-SNI mice (2 males, 2 females) were quantified (Fig. 20A-G). Although the quantity of microglia differed between sham samples and the four defined regions, the number of microglia remained stable along the rostro-caudal axis in the 3 days post-sham samples from male and female mice (Fig. 20A-C). Three days post-SNI, an increase in the number of microglia in both the dorsal and ventral horns ipsilateral to injury was observed (Fig. 20D-G). However, a distinct pattern was noticed between males and females. Female microglia density increased similarly in the dorsal and ventral horns ipsilateral to the injury, whereas male microglia peaked more rostrally in the ventral horn and more caudally in the dorsal horn. This finding suggests broader male-specific microgliosis on the rostral-caudal axis in the ventral horn as compared to the dorsal horn. The data shown here represent preliminary results obtained while establishing the technique and evaluating different technologies (endogenous expression of tdTomato in microglia, tissue clearing, light-

sheet microscopy, and image analysis using Imaris). Further work should be performed to confirm these findings with a larger sample size.

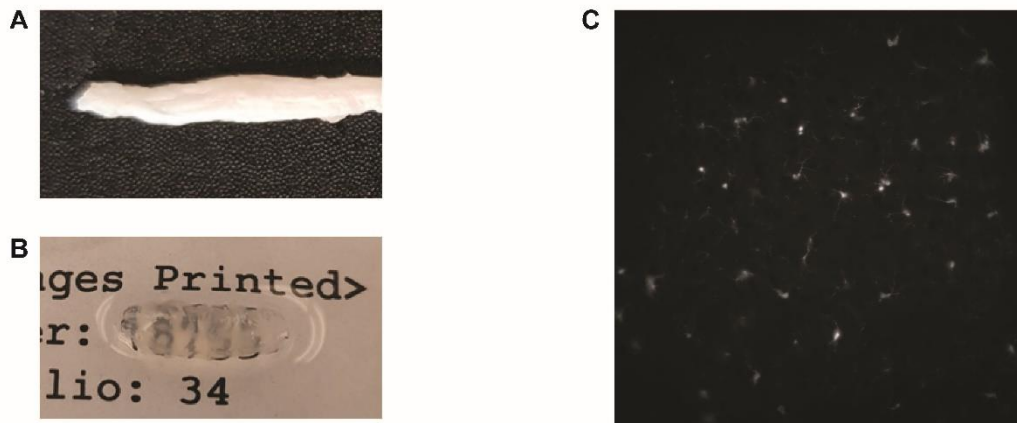


Figure 17. Clearing and imaging of mouse spinal cord. Mouse spinal cord **A)** before and **B)** after clearing with the X-Clarity Tissue clearing system. **C)** Microglia from a $Tmem119^{creERT2/+}; Ai14^{tdTomato/+}$ mouse imaged with LSM, original magnification X20.

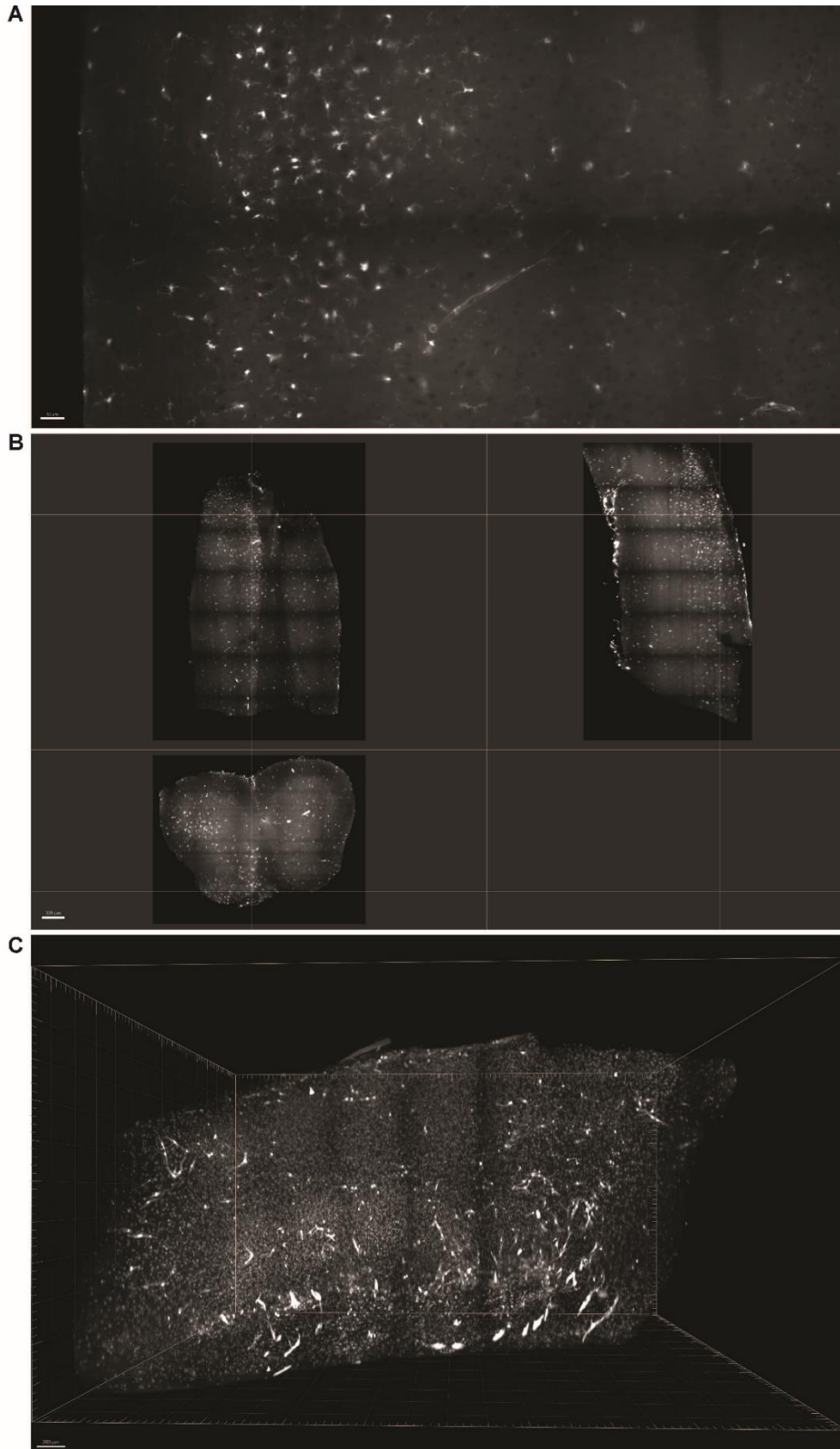


Figure 18. Fluorescently labeled microglia in the spinal cord. A) Stack showing fluorescently labeled microglia at 100% zoom. **B)** Coronal, transverse, and sagittal views of the spinal cord of a female mouse 3 days post-SNI. **C)** Side view of a 3D reconstruction of a XCLARITY-processed spinal cord imaged by LSFM showing fluorescently labeled microglia in a 3 days post-SNI female mouse.

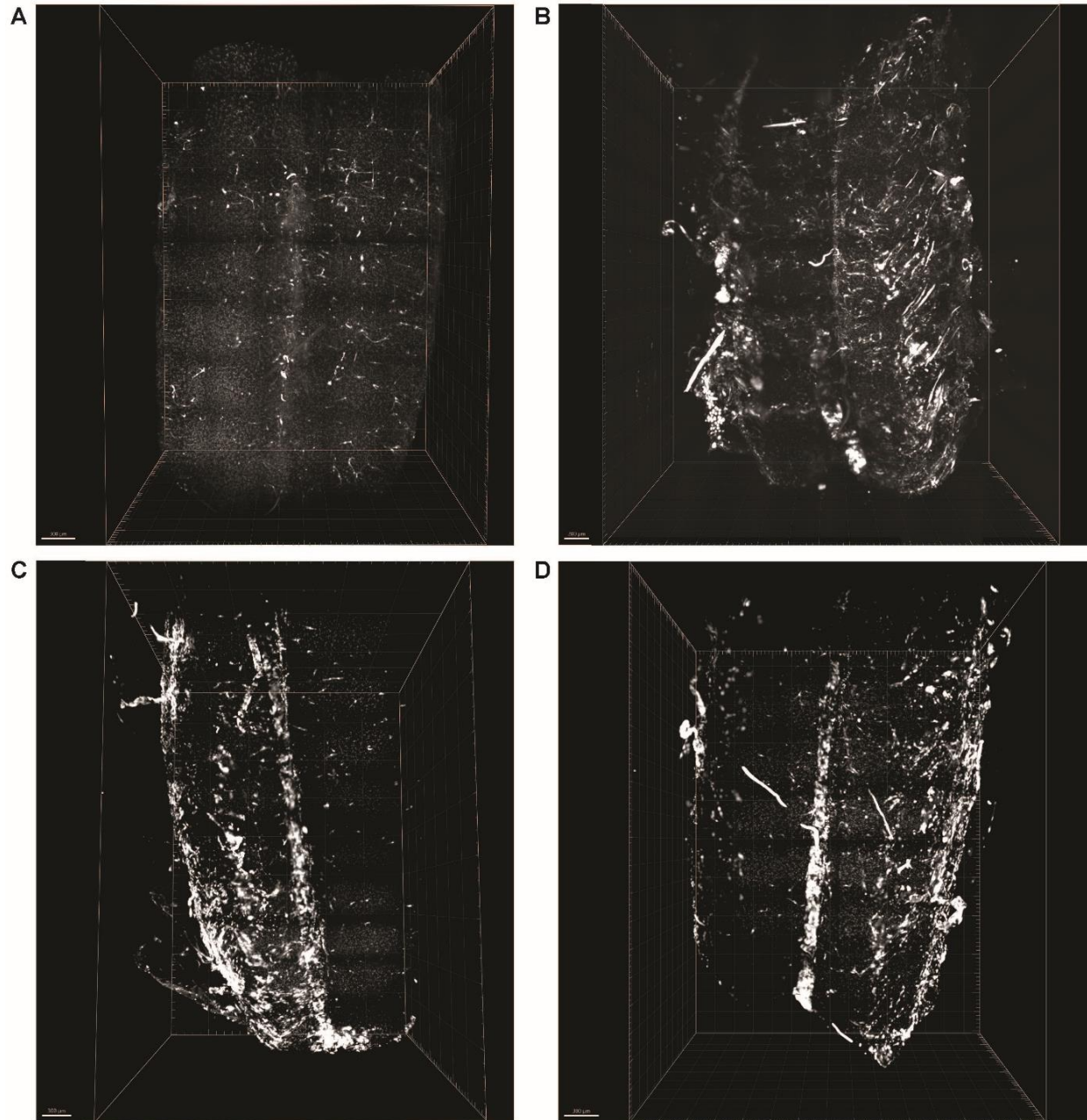


Figure 19. 3D reconstruction of mouse lumbar spinal cord of *Tmem119cre^{ERT2/+}; Ai14^{tdTomato/+}* mice. Coronal view showing fluorescently labeled microglia in 3 days post-SNI **A)** female and **B)** male mice. **C)** and **D)** correspond to 3 days post-sham female and male samples, respectively. The approximate size of each sample can be found in Appendix C Table C1.

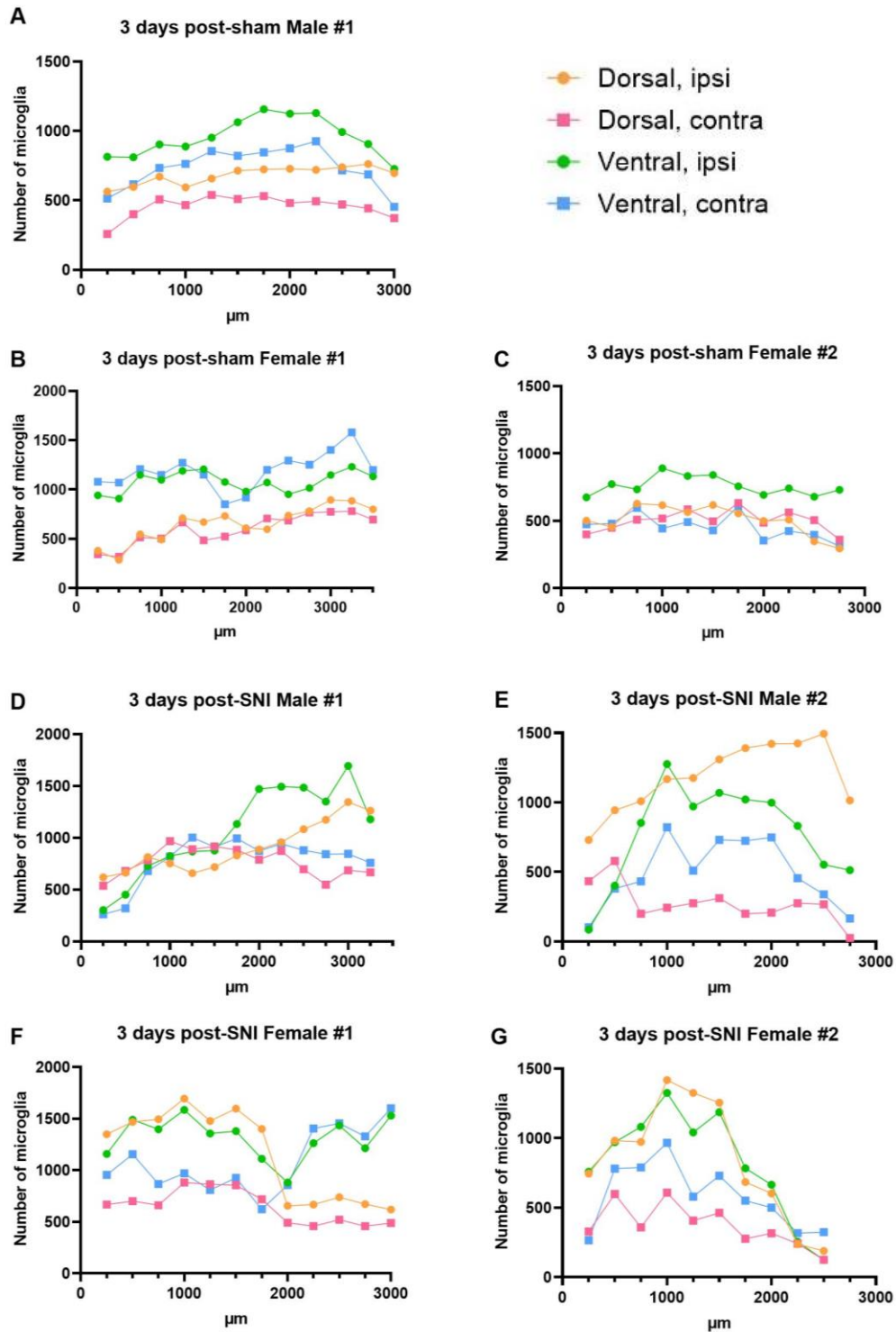


Figure 20. Quantification of microglia in the lumbar region of cleared mouse spinal cord. Microglia detected as spots in 3 days post-sham **A)** male and **B, C)** females, and 3 days post-SNI **D, E)** males and **F, G)** females. Numbers correspond to microglia detected in bins defined every 250 μ m in the lumbar region of the spinal cord.

4. Discussion

4.1 Single-cell RNA sequencing of spinal microglia reveals transcriptional heterogeneity after peripheral nerve injury

Using single-cell RNA sequencing, we studied the heterogeneity of microglia in the mouse spinal cord and analyzed microglial responses to peripheral nerve injury in male and female mice at three different time points by transcriptionally profiling a large number of cells. Single-cell transcriptomics revealed that microglia from the mouse spinal cord exists in heterogeneous subpopulations. Unsupervised clustering of scRNAseq data revealed that most microglia in mice belong to six different clusters (1-6), which represents ~98% of all microglia in naive animals. We also detected other small populations of vessel-associated microglia (cluster 10) and perivascular macrophages (cluster 11). Peripheral nerve injury led to an increase in the proportion of two clusters of proliferating microglia (clusters 7 and 8), as well as the appearance of a male-specific microglial subtype (cluster 9). High throughput scRNAseq experiments use droplet microfluidics to isolate cells. The droplets containing single cells and mRNA capture beads can sometimes be filled with two cells, which is known as doublets.⁽⁸⁹⁾ This technical artifact can produce misleading results because doublets that contain cells with distinct transcriptional states (called heterotypic doublets) would lead to aberrant differential expression and clustering analysis.⁽⁹⁰⁾ Since cells in cluster 10 expressed microglial markers as well as genes expressed by endothelial cells such as *Cldn5* and *Pecam1*, it is a possibility that these cells represent doublets. The same case applies to cluster 11, which contains cells expressing microglial and macrophage markers (*Mgl2*, *Mrc1*). In addition, we sequenced a high number of cells, which

translates into a higher doublet rate formation. However, doublet analysis on our scRNAseq data showed that only 12.21% of cells in cluster 10 and 17.1% in Cluster 11 represent doublets (Fig. B1A). Correlation analysis of DEGs of singlets from cluster 10 versus all the cells in the cluster (singlets + doublets) resulted in an $r=1$ (Fig. B1B). We obtained the same result after correlation analysis of singlets from cluster 11 (Fig. B1C). It demonstrates that single microglia in clusters 10 and 11 express the cluster markers established before doublet analysis.

Additionally, Niehaus et. al. uncovered a population of MRC1⁺ spinal cord macrophages that proliferate in the dorsal horn in response to a superficial injury (sham surgery), as well as attenuate microgliosis and resolve mechanical pain after sham surgery, effect that is not seen in SNI animals.⁽⁹¹⁾ *Mrc1* appeared as one of the top markers for cluster 11. Similar to their results, we see a higher proportion of cluster 11 microglia in males 14 days post-sham (0.745%) than in post-SNI mice (0.46%). It is worth mentioning that their study was performed exclusively in male mice, but we see a similar tendency in female mice (0.71% of cluster 11 microglia 14 days post-sham vs 0.4% in post-SNI mice). Further experiments are needed to confirm a role for these cells in the response to superficial injury and pain development in female mice.

The identification of uniquely expressed genes in seven of the eleven microglial clusters allows for further experiments to define the spatial distribution of the different subpopulations of microglia.

4.2 Sex-specific changes in the transcriptome of microglia after peripheral nerve injury

As previously shown in several studies, we found that in male mice, microglia display a strong inflammatory response at the acute phase (day 3) following peripheral nerve injury. The large number of DEGs registered at day 3 decreased over time. The predominant biological processes found in GO analysis at day 14 and 5 months post-SNI included metabolic processes such as energy production and lipid metabolism. Overall, these results indicate that after the initial immune response to injury, microglial transcriptomic landscape changes from an immune-reactive state towards a metabolically altered state. This effect has been previously seen in microglia in pathologies including AD and MS(92), and macrophages in response to damage(93), showing that microglia move to glycolysis instead of mitochondrial oxidative phosphorylation for ATP production(94, 95), and upregulate genes related to lipid and lipoprotein metabolism(96). Compared to male mice, females displayed weaker inflammatory responses at day three, showing endocytosis as one of the top processes. Many of the DEGs found at day 3 post-SNI in male microglia were genes coding for ribosomal proteins (*Rpl* and *Rps*). This phenomenon was not observed in female microglia. The increased expression of these genes could lead to an upregulation in ribosomal proteins and further enhance the capacity of the cells to produce new proteins required for the activation or maintenance of microglia functions.(97) At an early time point, microglia in males show downregulation of MAPK phosphatases *Dusp1* and *Dusp6*, negative regulators of the inflammatory response(98, 99), and upregulation of *Dusp2*, which function as a positive regulator of inflammation(100),

indicating an overall pro-inflammatory response; while in females, downregulation of *Dusp2* and upregulation of *Dusp6* reflect an anti-inflammatory state. The downregulation 3 days post-SNI of *Dusp6*, an ERK-directed phosphatase, agrees with previous findings of ERK pathway activation in microglia after nerve injury.(101, 102) Even more, the downregulation of *Dusp1* and *Dusp6* exclusively in males is consistent with the male-specific upregulation of p38 phosphorylation(69) that is key to the activation of microglia after nerve injury.(103, 104) Since p38 MAPKs induce the expression of Tumor necrosis factor (TNF) in microglia following peripheral nerve injury(61), it is not surprising that we found an upregulation of TNF in most of the microglia clusters exclusively in male mice. Studies that show the role of TNF in the development of neuropathic pain have utilized male rats or mice(61, 105). The fact that we do not see a change in the expression of TNF or interleukin (IL)-1 β in female mice points to possible sex differences in the mechanisms underlying the development and maintenance of neuropathic pain.

In addition to differences in the DEGs present in several clusters in males and females after peripheral nerve injury, we found a subpopulation of microglia (cluster 9) detected only at day 3 post-SNI and exclusively in males. This cluster shows a strong inflammatory profile that is highly similar to the IRM signature. Out of the 83 DEGs shared between the IRM signature and the male-specific cluster, 56 DEGs correspond to upregulated *Rp* genes. Twenty-one of the remaining 27 DEGs are upregulated in the IRM signature but downregulated in cluster 9. The similarity between these two transcriptional states may be driven by the need to produce more proteins. Since the IRM signature was found after the study of male mice in a model of multiple sclerosis

(MS), and it showed a high correlation with a male-specific cluster in our work, further research on MS using male and female mice is required given the higher prevalence of this disease in women.(106) Among the upregulated DEGs shared between the IRM signature and cluster 9, we found the chemokine *Cxcl16*. Although *Cxcl16* is a marker for clusters 5, 7, and 9, it appeared as a DEG at day 3 post-SNI exclusively in males in clusters 1, 2, 7, 8, and 9, with a higher expression in the latest. It has been shown that CXCL16 can modulate the activity of GABAergic and glutamatergic synapses in the CA1 area in a microglia-dependent manner that involves the adenosine receptor type 3 (A3R).(107) A3R agonists reversed the neuropathic pain induced with the chronic constriction injury (CCI) model in male rats and mice.(108) It would be interesting to test the effect of microglial CXCL16 in the development of neuropathic pain in male and female mice.

4.3 Peripheral nerve injury induces greater proliferation of microglia in the lumbar spinal cord of male mice as compared to female mice

Even though males and females display similar levels of microgliosis in response to peripheral nerve injury, we found that microglia proliferate more in male mice when compared to females at day 3 post-SNI. Although we saw an upregulation in the expression of genes related to apoptosis in male microglia at day 3 post-SNI, co-immunostaining of an apoptotic marker (CC3) and microglia (IBA1) did not show cells undergoing apoptosis at that time point, which rules out cell death as the mechanism that leads to equal microgliosis in males and females. Another possible explanation is that female microglia proliferate before male microglia. Looking at Ki67 staining in

microglia at earlier time points (e.g., day 1 and day 2 post-SNI) would answer this question.

4.4 APOE is upregulated in spinal microglia at chronic phases of neuropathic pain

The scRNAseq data unveiled an upregulation in the expression levels of *ApoE* mRNA across most clusters at late time points (day 14 and 5 months) but not at the acute phase (day 3) following nerve injury. *ApoE* appeared as the top upregulated gene in many clusters on day 14 and month 5. A significant increase in APOE protein levels was also present on day 14 and month 5 post-SNI. Microglia accumulate cholesterol following phagocytosis of apoptotic cells and myelin debris. APOE could take part in the removal of intracellular cholesterol from microglia. Microglia use lipids as a source of energy, via oxidative metabolism, and as precursors of several inflammatory mediators. Thus, the regulation of lipid metabolism by APOE could contribute to the energy production and inflammatory activity of microglia. The proposal of the role of APOE in pain is not new.(109) In addition, it was recently shown that Apolipoprotein A-I binding protein (AIBP) removes cholesterol excess from the plasma membrane and leads to a reduction in inflammatory signaling.(110) Even more, intrathecal injections of AIBP reversed allodynia in chemotherapeutic cisplatin-induced neuropathic pain and following intraplantar formalin and intrathecal LPS.(110) Further experiments are needed to elucidate the functions of APOE in cholesterol efflux from microglia after nerve injury and the effect on the development and or maintenance of neuropathic pain.

4.5 LYVE-1 positive cells are observed in the lumbar spinal cord in proximity to blood vessels

We reported the presence of TMEM119 positive cells covering the surface of the spinal cord. Furthermore, we detected LYVE1+ IBA1+ tdTomato+ cells in proximity to blood vessels in the spinal cord of Tmem119creERT2/+; Ai14tdTomato/+ mouse. It has been shown that peripheral nerve injury in rats leads to leakage of the blood-spinal cord barrier (BSCB), which contributes to the influx of inflammatory cytokines that cause neuropathic pain.(111) It would be interesting to explore the contribution of LYVE1 positive cells to the integrity of the BSCB, especially after peripheral nerve injury.

4.6 3D imaging of microglia using light-sheet microscopy

After peripheral nerve injury, male and female mice display similar levels of microgliosis. However, male mice showed increased proliferation 3 days post-SNI. Cleared spinal cord coupled with LSFM could be used for descriptive and quantitative studies of microglia. 3D imaging of cleared lumbar spinal cord of Tmem119-CreERT2: Ai14 mice revealed different microgliosis patterns in males and females 3 days post-SNI. The differences in the gliosis could indicate variations in cell migration contributing to the equal microgliosis but different cell proliferation post-SNI. Nonetheless, the processing of 3D images, especially the filtering criteria to quantify microglia, should be optimized to directly compare numbers between different samples.

Some of the samples display prominent expression of tdTomato on the surface of the spinal cords and structures that resemble blood vessels (Fig. 19C, Appendix C Fig. C1A and C). These samples were processed with the meninges attached. As previously mentioned, it has been reported that TMEM119 is expressed in leptomeningeal cells

that border the brain surface and penetrate it, ensheathing large blood vessels.(86) This would explain the layer of cells expressing TMEM119 on the surface of the spinal cord. Depending on the purpose of the study, the spinal cord meninges could be maintained or removed to facilitate imaging and image analysis.

Conclusion

Our dataset presents a comprehensive characterization of mouse spinal cord microglia heterogeneity. It sets the basis to investigate the function of specific subpopulations of microglia and transcriptional states in chronic pain and other spinal cord pathologies.

Furthermore, the results of this study provide evidence for sex-specific responses of microglia to peripheral nerve injury. At an early time point, we found an increased proliferation of microglia in male mice when compared to females, upregulation of ribosomal protein genes expression in males, and differences in the pattern of microgliosis. The identification of a male-specific microglia subpopulation with a marked inflammatory profile might allow a better understanding of sex-specific pain mechanisms and the development of targeted therapies. We observed a switch from an immune to an altered metabolic state of microglia. This switch might be a potential mechanism behind neuropathic pain development and maintenance. The upregulation of APOE could play a role in this metabolic alteration. Additional studies on the function of APOE and LYVE1 / IBA1-positive cells in the mouse spinal cord might provide insights into the microglia-dependent mechanisms of neuropathic pain.

References

1. Raja SN, Carr DB, Cohen M, Finnerup NB, Flor H, Gibson S, et al. The revised International Association for the Study of Pain definition of pain: concepts, challenges, and compromises. *Pain*. 2020;161(9):1976-82.
2. Woolf CJ. What is this thing called pain? *J Clin Invest*. 2010;120(11):3742-4.
3. Wieseler-Frank J, Maier SF, Watkins LR. Glial activation and pathological pain. *Neurochem Int*. 2004;45(2-3):389-95.
4. Jensen TS, Baron R, Haanpaa M, Kalso E, Loeser JD, Rice ASC, et al. A new definition of neuropathic pain. *Pain*. 2011;152(10):2204-5.
5. Colloca L, Ludman T, Bouhassira D, Baron R, Dickenson AH, Yarnitsky D, et al. Neuropathic pain. *Nat Rev Dis Primers*. 2017;3:17002.
6. Cavalli E, Mammanna S, Nicoletti F, Bramanti P, Mazzon E. The neuropathic pain: An overview of the current treatment and future therapeutic approaches. *Int J Immunopathol Pharmacol*. 2019;33:2058738419838383.
7. van Hecke O, Austin SK, Khan RA, Smith BH, Torrance N. Neuropathic pain in the general population: a systematic review of epidemiological studies. *Pain*. 2014;155(4):654-62.
8. Finnerup NB, Attal N, Haroutounian S, McNicol E, Baron R, Dworkin RH, et al. Pharmacotherapy for neuropathic pain in adults: a systematic review and meta-analysis. *Lancet Neurol*. 2015;14(2):162-73.
9. Finnerup NB, Kuner R, Jensen TS. Neuropathic Pain: From Mechanisms to Treatment. *Physiol Rev*. 2021;101(1):259-301.
10. Kyranou M, Puntillo K. The transition from acute to chronic pain: might intensive care unit patients be at risk? *Ann Intensive Care*. 2012;2(1):36.
11. Treede RD, Rief W, Barke A, Aziz Q, Bennett MI, Benoliel R, et al. A classification of chronic pain for ICD-11. *Pain*. 2015;156(6):1003-7.
12. McGreevy K, Bottros MM, Raja SN. Preventing Chronic Pain following Acute Pain: Risk Factors, Preventive Strategies, and their Efficacy. *Eur J Pain Suppl*. 2011;5(2):365-72.
13. Feizerfan A, Sheh G. Transition from acute to chronic pain. *Continuing Education in Anaesthesia, Critical Care & Pain*. 2015;15(2):98-102.
14. Colleoni M, Sacerdote P. Murine models of human neuropathic pain. *Biochim Biophys Acta*. 2010;1802(10):924-33.
15. Mogil JS, Davis KD, Derbyshire SW. The necessity of animal models in pain research. *Pain*. 2010;151(1):12-7.
16. Jaggi AS, Jain V, Singh N. Animal models of neuropathic pain. *Fundam Clin Pharmacol*. 2011;25(1):1-28.
17. Mogil JS. Animal models of pain: progress and challenges. *Nat Rev Neurosci*. 2009;10(4):283-94.
18. Decosterd I, Woolf CJ. Spared nerve injury: an animal model of persistent peripheral neuropathic pain. *Pain*. 2000;87(2):149-58.
19. Challa SR. Surgical animal models of neuropathic pain: Pros and Cons. *Int J Neurosci*. 2015;125(3):170-4.
20. Hill R. NK1 (substance P) receptor antagonists--why are they not analgesic in humans? *Trends Pharmacol Sci*. 2000;21(7):244-6.
21. Percie du Sert N, Rice AS. Improving the translation of analgesic drugs to the clinic: animal models of neuropathic pain. *Br J Pharmacol*. 2014;171(12):2951-63.
22. Berge OG. Predictive validity of behavioural animal models for chronic pain. *Br J Pharmacol*. 2011;164(4):1195-206.
23. Deuis JR, Dvorakova LS, Vetter I. Methods Used to Evaluate Pain Behaviors in Rodents. *Front Mol Neurosci*. 2017;10:284.

24. Gregory NS, Harris AL, Robinson CR, Dougherty PM, Fuchs PN, Sluka KA. An overview of animal models of pain: disease models and outcome measures. *J Pain*. 2013;14(11):1255-69.
25. Langford DJ, Bailey AL, Chanda ML, Clarke SE, Drummond TE, Echols S, et al. Coding of facial expressions of pain in the laboratory mouse. *Nat Methods*. 2010;7(6):447-9.
26. Yam MF, Loh YC, Tan CS, Khadijah Adam S, Abdul Manan N, Basir R. General Pathways of Pain Sensation and the Major Neurotransmitters Involved in Pain Regulation. *Int J Mol Sci*. 2018;19(8).
27. Basbaum AI, Bautista DM, Scherrer G, Julius D. Cellular and molecular mechanisms of pain. *Cell*. 2009;139(2):267-84.
28. Kuner R. Central mechanisms of pathological pain. *Nat Med*. 2010;16(11):1258-66.
29. Stucky CL, Gold MS, Zhang X. Mechanisms of pain. *Proc Natl Acad Sci U S A*. 2001;98(21):11845-6.
30. Woolf CJ, Ma Q. Nociceptors--noxious stimulus detectors. *Neuron*. 2007;55(3):353-64.
31. Rosen S, Ham B, Mogil JS. Sex differences in neuroimmunity and pain. *J Neurosci Res*. 2017;95(1-2):500-8.
32. Ruau D, Liu LY, Clark JD, Angst MS, Butte AJ. Sex differences in reported pain across 11,000 patients captured in electronic medical records. *J Pain*. 2012;13(3):228-34.
33. Bartley EJ, Fillingim RB. Sex differences in pain: a brief review of clinical and experimental findings. *Br J Anaesth*. 2013;111(1):52-8.
34. Mogil JS. Qualitative sex differences in pain processing: emerging evidence of a biased literature. *Nat Rev Neurosci*. 2020;21(7):353-65.
35. Mogil JS, Bailey AL. Sex and gender differences in pain and analgesia. *Prog Brain Res*. 2010;186:141-57.
36. Fillingim RB, Kaplan L, Staud R, Ness TJ, Glover TL, Campbell CM, et al. The A118G single nucleotide polymorphism of the mu-opioid receptor gene (OPRM1) is associated with pressure pain sensitivity in humans. *J Pain*. 2005;6(3):159-67.
37. Valverde P, Healy E, Jackson I, Rees JL, Thody AJ. Variants of the melanocyte-stimulating hormone receptor gene are associated with red hair and fair skin in humans. *Nat Genet*. 1995;11(3):328-30.
38. Miaskowski C, Levine JD. Does opioid analgesia show a gender preference for females? *Pain Forum*. 1999;8(1):34-44.
39. Kettenmann H, Hanisch UK, Noda M, Verkhratsky A. Physiology of microglia. *Physiol Rev*. 2011;91(2):461-553.
40. Ginhoux F, Greter M, Leboeuf M, Nandi S, See P, Gokhan S, et al. Fate mapping analysis reveals that adult microglia derive from primitive macrophages. *Science*. 2010;330(6005):841-5.
41. Masuda T, Sankowski R, Staszewski O, Prinz M. Microglia Heterogeneity in the Single-Cell Era. *Cell Rep*. 2020;30(5):1271-81.
42. Askew K, Li K, Olmos-Alonso A, Garcia-Moreno F, Liang Y, Richardson P, et al. Coupled Proliferation and Apoptosis Maintain the Rapid Turnover of Microglia in the Adult Brain. *Cell Rep*. 2017;18(2):391-405.
43. Stratoulia V, Venero JL, Tremblay ME, Joseph B. Microglial subtypes: diversity within the microglial community. *EMBO J*. 2019;38(17):e101997.
44. Kettenmann H, Kirchhoff F, Verkhratsky A. Microglia: new roles for the synaptic stripper. *Neuron*. 2013;77(1):10-8.
45. Pocock JM, Piers TM. Modelling microglial function with induced pluripotent stem cells: an update. *Nat Rev Neurosci*. 2018;19(8):445-52.
46. Prinz M, Jung S, Priller J. Microglia Biology: One Century of Evolving Concepts. *Cell*. 2019;179(2):292-311.

47. Wolf SA, Boddeke HW, Kettenmann H. Microglia in Physiology and Disease. *Annu Rev Physiol.* 2017;79:619-43.
48. Ransohoff RM, Perry VH. Microglial physiology: unique stimuli, specialized responses. *Annu Rev Immunol.* 2009;27:119-45.
49. Jurga AM, Paleczna M, Kuter KZ. Overview of General and Discriminating Markers of Differential Microglia Phenotypes. *Front Cell Neurosci.* 2020;14:198.
50. Martinez FO, Gordon S. The M1 and M2 paradigm of macrophage activation: time for reassessment. *F1000Prime Rep.* 2014;6:13.
51. Orihuela R, McPherson CA, Harry GJ. Microglial M1/M2 polarization and metabolic states. *Br J Pharmacol.* 2016;173(4):649-65.
52. Ransohoff RM. A polarizing question: do M1 and M2 microglia exist? *Nat Neurosci.* 2016;19(8):987-91.
53. Schwarz JM, Sholar PW, Bilbo SD. Sex differences in microglial colonization of the developing rat brain. *J Neurochem.* 2012;120(6):948-63.
54. Weinhard L, Neniskyte U, Vadasiute A, di Bartolomei G, Aygun N, Riviere L, et al. Sexual dimorphism of microglia and synapses during mouse postnatal development. *Dev Neurobiol.* 2018;78(6):618-26.
55. Hammond TR, Dufort C, Dissing-Olesen L, Giera S, Young A, Wysoker A, et al. Single-Cell RNA Sequencing of Microglia throughout the Mouse Lifespan and in the Injured Brain Reveals Complex Cell-State Changes. *Immunity.* 2019;50(1):253-71 e6.
56. Villa A, Gelosa P, Castiglioni L, Cimino M, Rizzi N, Pepe G, et al. Sex-Specific Features of Microglia from Adult Mice. *Cell Rep.* 2018;23(12):3501-11.
57. Masuda T, Sankowski R, Staszewski O, Bottcher C, Amann L, Sagar, et al. Spatial and temporal heterogeneity of mouse and human microglia at single-cell resolution. *Nature.* 2019;566(7744):388-92.
58. Keren-Shaul H, Spinrad A, Weiner A, Matcovitch-Natan O, Dvir-Szternfeld R, Ulland TK, et al. A Unique Microglia Type Associated with Restricting Development of Alzheimer's Disease. *Cell.* 2017;169(7):1276-90 e17.
59. Sousa C, Golebiewska A, Poovathingal SK, Kaoma T, Pires-Afonso Y, Martina S, et al. Single-cell transcriptomics reveals distinct inflammation-induced microglia signatures. *EMBO Rep.* 2018;19(11).
60. Jordao MJC, Sankowski R, Brendecke SM, Sagar, Locatelli G, Tai YH, et al. Single-cell profiling identifies myeloid cell subsets with distinct fates during neuroinflammation. *Science.* 2019;363(6425).
61. Inoue K, Tsuda M. Microglia in neuropathic pain: cellular and molecular mechanisms and therapeutic potential. *Nat Rev Neurosci.* 2018;19(3):138-52.
62. Tsuda M, Shigemoto-Mogami Y, Koizumi S, Mizokoshi A, Kohsaka S, Salter MW, et al. P2X4 receptors induced in spinal microglia gate tactile allodynia after nerve injury. *Nature.* 2003;424(6950):778-83.
63. Jin SX, Zhuang ZY, Woolf CJ, Ji RR. p38 mitogen-activated protein kinase is activated after a spinal nerve ligation in spinal cord microglia and dorsal root ganglion neurons and contributes to the generation of neuropathic pain. *J Neurosci.* 2003;23(10):4017-22.
64. Zhao H, Alam A, Chen Q, M AE, Pal A, Eguchi S, et al. The role of microglia in the pathobiology of neuropathic pain development: what do we know? *Br J Anaesth.* 2017;118(4):504-16.
65. Mapplebeck JC, Beggs S, Salter MW. Molecules in pain and sex: a developing story. *Mol Brain.* 2017;10(1):9.
66. Chen G, Zhang YQ, Qadri YJ, Serhan CN, Ji RR. Microglia in Pain: Detrimental and Protective Roles in Pathogenesis and Resolution of Pain. *Neuron.* 2018;100(6):1292-311.

67. Sorge RE, LaCroix-Fralish ML, Tuttle AH, Sotocinal SG, Austin JS, Ritchie J, et al. Spinal cord Toll-like receptor 4 mediates inflammatory and neuropathic hypersensitivity in male but not female mice. *J Neurosci*. 2011;31(43):15450-4.
68. Sorge RE, Mapplebeck JC, Rosen S, Beggs S, Taves S, Alexander JK, et al. Different immune cells mediate mechanical pain hypersensitivity in male and female mice. *Nat Neurosci*. 2015;18(8):1081-3.
69. Taves S, Berta T, Liu DL, Gan S, Chen G, Kim YH, et al. Spinal inhibition of p38 MAP kinase reduces inflammatory and neuropathic pain in male but not female mice: Sex-dependent microglial signaling in the spinal cord. *Brain Behav Immun*. 2016;55:70-81.
70. Inyang KE, Szabo-Pardi T, Wentworth E, McDougal TA, Dussor G, Burton MD, et al. The antidiabetic drug metformin prevents and reverses neuropathic pain and spinal cord microglial activation in male but not female mice. *Pharmacol Res*. 2019;139:1-16.
71. Butovsky O, Jedrychowski MP, Moore CS, Cialic R, Lanser AJ, Gabriely G, et al. Identification of a unique TGF-beta-dependent molecular and functional signature in microglia. *Nat Neurosci*. 2014;17(1):131-43.
72. Jiang ZH, Peng J, Yang HL, Fu XL, Wang JZ, Liu L, et al. Upregulation and biological function of transmembrane protein 119 in osteosarcoma. *Exp Mol Med*. 2017;49(5):e329.
73. Chen G, Ning B, Shi T. Single-Cell RNA-Seq Technologies and Related Computational Data Analysis. *Front Genet*. 2019;10:317.
74. McKinnon KM. Flow Cytometry: An Overview. *Curr Protoc Immunol*. 2018;120:5 1 -5 1 11.
75. Li Q, Cheng Z, Zhou L, Darmanis S, Neff NF, Okamoto J, et al. Developmental Heterogeneity of Microglia and Brain Myeloid Cells Revealed by Deep Single-Cell RNA Sequencing. *Neuron*. 2019;101(2):207-23 e10.
76. Guneykaya D, Ivanov A, Hernandez DP, Haage V, Wojtas B, Meyer N, et al. Transcriptional and Translational Differences of Microglia from Male and Female Brains. *Cell Rep*. 2018;24(10):2773-83 e6.
77. Mogil JS. Sex differences in pain and pain inhibition: multiple explanations of a controversial phenomenon. *Nat Rev Neurosci*. 2012;13(12):859-66.
78. Shields SD, Eckert WA, 3rd, Basbaum AI. Spared nerve injury model of neuropathic pain in the mouse: a behavioral and anatomic analysis. *J Pain*. 2003;4(8):465-70.
79. Chen EY, Tan CM, Kou Y, Duan Q, Wang Z, Meirelles GV, et al. Enrichr: interactive and collaborative HTML5 gene list enrichment analysis tool. *BMC Bioinformatics*. 2013;14:128.
80. Kuleshov MV, Jones MR, Rouillard AD, Fernandez NF, Duan Q, Wang Z, et al. Enrichr: a comprehensive gene set enrichment analysis web server 2016 update. *Nucleic Acids Res*. 2016;44(W1):W90-7.
81. Xie Z, Bailey A, Kuleshov MV, Clarke DJB, Evangelista JE, Jenkins SL, et al. Gene Set Knowledge Discovery with Enrichr. *Curr Protoc*. 2021;1(3):e90.
82. Higashimori H, Schin CS, Chiang MS, Morel L, Shoneye TA, Nelson DL, et al. Selective Deletion of Astroglial FMRP Dysregulates Glutamate Transporter GLT1 and Contributes to Fragile X Syndrome Phenotypes In Vivo. *J Neurosci*. 2016;36(27):7079-94.
83. Haruwaka K, Ikegami A, Tachibana Y, Ohno N, Konishi H, Hashimoto A, et al. Dual microglia effects on blood brain barrier permeability induced by systemic inflammation. *Nat Commun*. 2019;10(1):5816.
84. Polgar E, Hughes DI, Arham AZ, Todd AJ. Loss of neurons from laminae I-III of the spinal dorsal horn is not required for development of tactile allodynia in the spared nerve injury model of neuropathic pain. *J Neurosci*. 2005;25(28):6658-66.
85. Yamazaki Y, Zhao N, Caulfield TR, Liu CC, Bu G. Apolipoprotein E and Alzheimer disease: pathobiology and targeting strategies. *Nat Rev Neurol*. 2019;15(9):501-18.
86. Kaiser T, Feng G. Tmem119-EGFP and Tmem119-CreERT2 Transgenic Mice for Labeling and Manipulating Microglia. *eNeuro*. 2019;6(4).

87. Kaser-Eichberger A, Schroedl F, Bieler L, Trost A, Bogner B, Runge C, et al. Expression of Lymphatic Markers in the Adult Rat Spinal Cord. *Front Cell Neurosci.* 2016;10:23.
88. Brezovakova V, Jadhav S. Identification of Lyve-1 positive macrophages as resident cells in meninges of rats. *J Comp Neurol.* 2020;528(12):2021-32.
89. McGinnis CS, Murrow LM, Gartner ZJ. DoubletFinder: Doublet Detection in Single-Cell RNA Sequencing Data Using Artificial Nearest Neighbors. *Cell Syst.* 2019;8(4):329-37 e4.
90. Bernstein NJ, Fong NL, Lam I, Roy MA, Hendrickson DG, Kelley DR. Solo: Doublet Identification in Single-Cell RNA-Seq via Semi-Supervised Deep Learning. *Cell Syst.* 2020;11(1):95-101 e5.
91. Niehaus JK, Taylor-Blake B, Loo L, Simon JM, Zylka MJ. Spinal macrophages resolve nociceptive hypersensitivity after peripheral injury. *Neuron.* 2021;109(8):1274-82 e6.
92. Baik SH, Kang S, Lee W, Choi H, Chung S, Kim JI, et al. A Breakdown in Metabolic Reprogramming Causes Microglia Dysfunction in Alzheimer's Disease. *Cell Metab.* 2019;30(3):493-507 e6.
93. Van den Bossche J, Saraber DL. Metabolic regulation of macrophages in tissues. *Cell Immunol.* 2018;330:54-9.
94. Mills EL, Kelly B, Logan A, Costa ASH, Varma M, Bryant CE, et al. Succinate Dehydrogenase Supports Metabolic Repurposing of Mitochondria to Drive Inflammatory Macrophages. *Cell.* 2016;167(2):457-70 e13.
95. Warburg O, Wind F, Negelein E. The Metabolism of Tumors in the Body. *J Gen Physiol.* 1927;8(6):519-30.
96. Loving BA, Bruce KD. Lipid and Lipoprotein Metabolism in Microglia. *Front Physiol.* 2020;11:393.
97. Denk F, Crow M, Didangelos A, Lopes DM, McMahon SB. Persistent Alterations in Microglial Enhancers in a Model of Chronic Pain. *Cell Rep.* 2016;15(8):1771-81.
98. Saha M, Skopelja S, Martinez E, Alvarez DL, Liponis BS, Romero-Sandoval EA. Spinal mitogen-activated protein kinase phosphatase-3 (MKP-3) is necessary for the normal resolution of mechanical allodynia in a mouse model of acute postoperative pain. *J Neurosci.* 2013;33(43):17182-7.
99. Ndong C, Landry RP, DeLeo JA, Romero-Sandoval EA. Mitogen activated protein kinase phosphatase-1 prevents the development of tactile sensitivity in a rodent model of neuropathic pain. *Mol Pain.* 2012;8:34.
100. Lang R, Hammer M, Mages J. DUSP meet immunology: dual specificity MAPK phosphatases in control of the inflammatory response. *J Immunol.* 2006;177(11):7497-504.
101. Obata K, Katsura H, Mizushima T, Sakurai J, Kobayashi K, Yamanaka H, et al. Roles of extracellular signal-regulated protein kinases 5 in spinal microglia and primary sensory neurons for neuropathic pain. *J Neurochem.* 2007;102(5):1569-84.
102. Calvo M, Zhu N, Grist J, Ma Z, Loeb JA, Bennett DL. Following nerve injury neuregulin-1 drives microglial proliferation and neuropathic pain via the MEK/ERK pathway. *Glia.* 2011;59(4):554-68.
103. Tsuda M, Mizokoshi A, Shigemoto-Mogami Y, Koizumi S, Inoue K. Activation of p38 mitogen-activated protein kinase in spinal hyperactive microglia contributes to pain hypersensitivity following peripheral nerve injury. *Glia.* 2004;45(1):89-95.
104. Luo X, Fitzsimmons B, Mohan A, Zhang L, Terrando N, Kordasiewicz H, et al. Intrathecal administration of antisense oligonucleotide against p38alpha but not p38beta MAP kinase isoform reduces neuropathic and postoperative pain and TLR4-induced pain in male mice. *Brain Behav Immun.* 2018;72:34-44.
105. Kawasaki Y, Zhang L, Cheng JK, Ji RR. Cytokine mechanisms of central sensitization: distinct and overlapping role of interleukin-1beta, interleukin-6, and tumor necrosis factor-

- alpha in regulating synaptic and neuronal activity in the superficial spinal cord. *J Neurosci.* 2008;28(20):5189-94.
106. Harbo HF, Gold R, Tintore M. Sex and gender issues in multiple sclerosis. *Ther Adv Neurol Disord.* 2013;6(4):237-48.
 107. Di Castro MA, Trettel F, Milior G, Maggi L, Ragozzino D, Limatola C. The chemokine CXCL16 modulates neurotransmitter release in hippocampal CA1 area. *Sci Rep.* 2016;6:34633.
 108. Ford A, Castonguay A, Cottet M, Little JW, Chen Z, Symons-Liguori AM, et al. Engagement of the GABA to KCC2 signaling pathway contributes to the analgesic effects of A3AR agonists in neuropathic pain. *J Neurosci.* 2015;35(15):6057-67.
 109. Dhillon H, Singh S. Role of Apolipoprotein E in the tangled mystery of pain. *Med Hypotheses.* 2018;114:58-64.
 110. Woller SA, Choi SH, An EJ, Low H, Schneider DA, Ramachandran R, et al. Inhibition of Neuroinflammation by AIBP: Spinal Effects upon Facilitated Pain States. *Cell Rep.* 2018;23(9):2667-77.
 111. Echeverry S, Shi XQ, Rivest S, Zhang J. Peripheral nerve injury alters blood-spinal cord barrier functional and molecular integrity through a selective inflammatory pathway. *J Neurosci.* 2011;31(30):10819-28.

Appendix A

Table A1. Cluster-specific markers for ISH experiments. Preliminary scRNAseq data was used to select cluster-specific markers for RNAscope probes. Clusters that were similar to the ones from the final analysis are indicated.

Cluster		Marker
Preliminary data	Final analysis	
2		<i>Srxn1</i>
4	4	<i>Ppm1n</i>
5	7,8	<i>Cdca3</i>
7	6	<i>Ifit1</i>
8		<i>Adgre5</i>
9	11	<i>Mrc1, Ccr2</i>
10	10	<i>Cldn5</i>

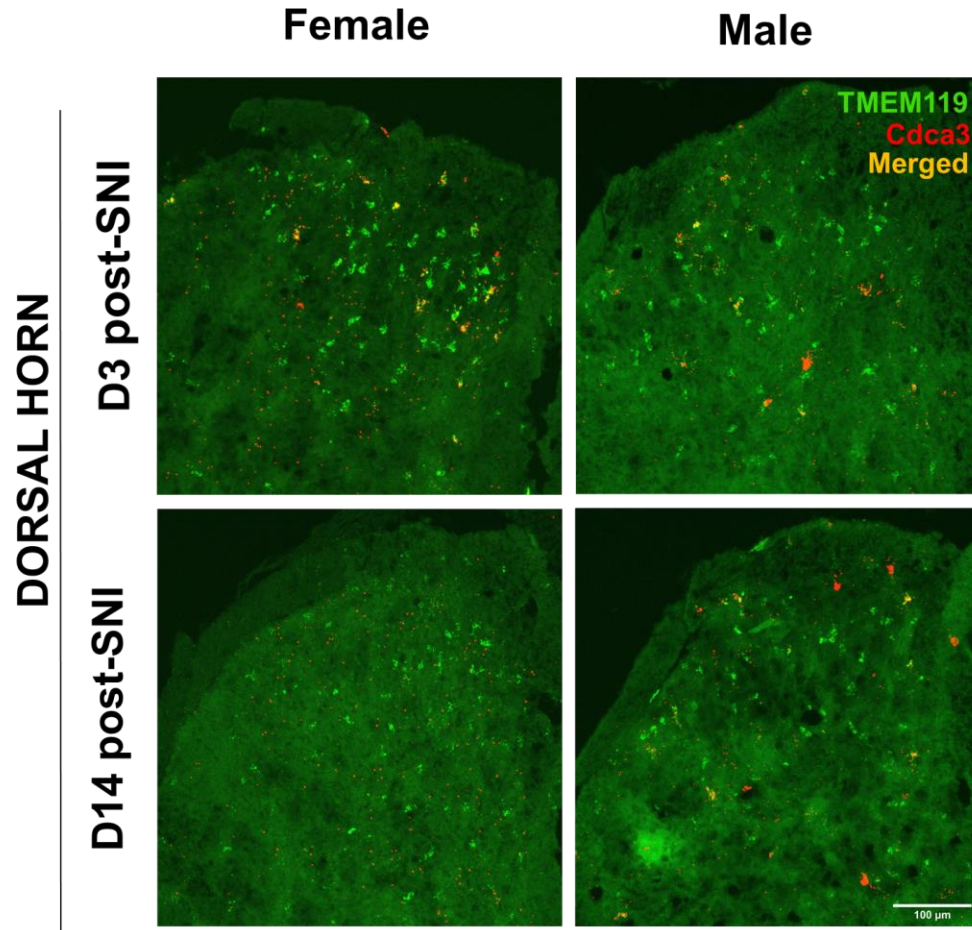


Figure A1. *Cdca3*-expressing microglia occupy the dorsal horn in a sex-dependent temporal manner after peripheral nerve injury. Z-stack confocal reconstructions of lumbar sections of the spinal cord dorsal horn hybridized with probes to *Cdca3* mRNA (red), and probes to *Tmem119* mRNA (green). Original magnification $\times 20$.

Appendix B

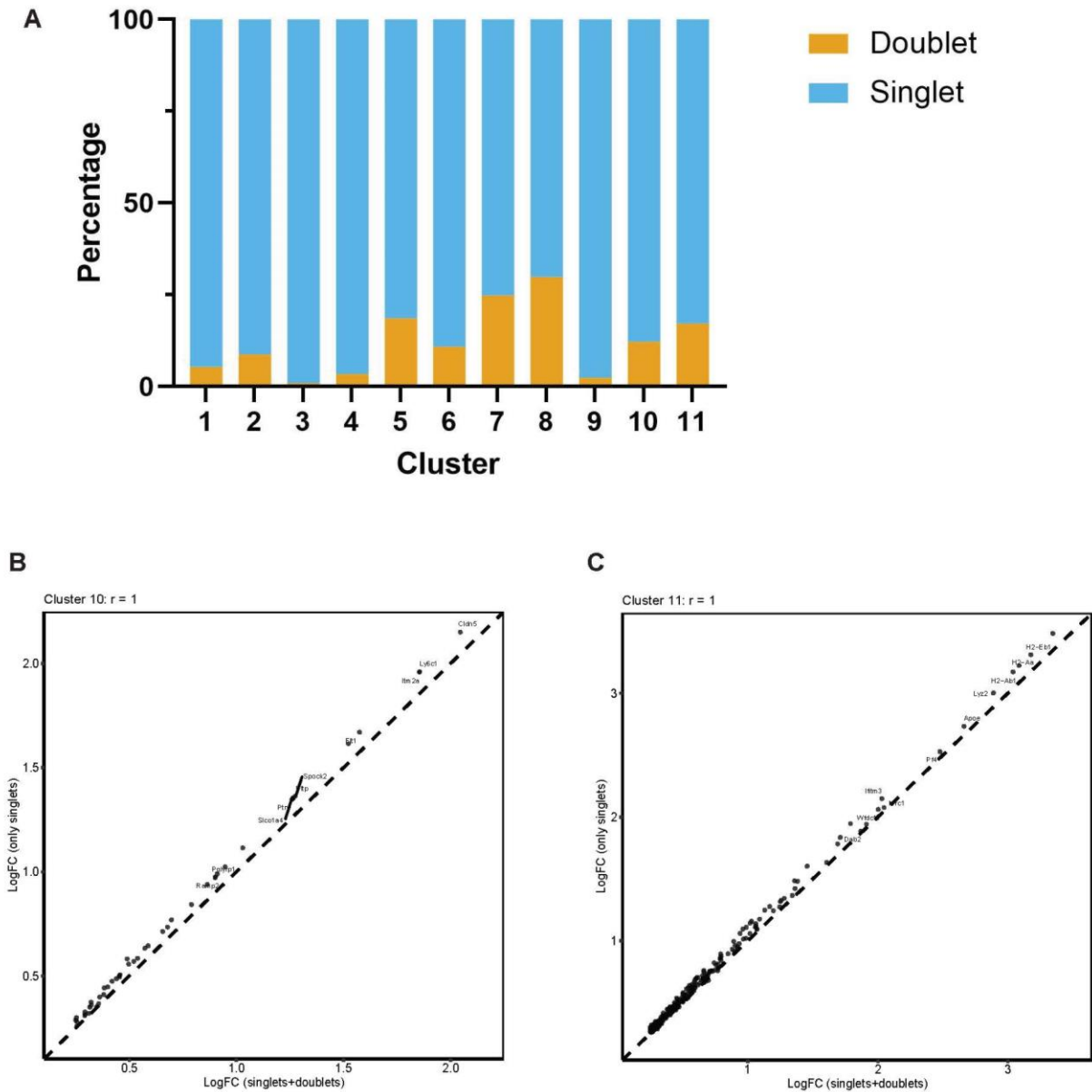


Figure B1. Doublet analysis of microglia scRNAseq dataset. **A)** Percentage of singlets and doublets present in each cluster and considered in the analysis of scRNAseq data from microglia. **B)** Fold change (LogFC) correlation of cluster 10 markers when singlets and doublets are considered vs singlets alone. Pearson correlation = 1. **C)** Fold change (LogFC) correlation of cluster 11 markers when singlets and doublets are considered vs singlets alone. Pearson correlation = 1.

Appendix C

Table C1. Approximate width and length of the imaged and quantified spinal cords.

Condition	Sample	Width (μm)	Length (μm)
3D post-SNI	F1	~2590	~3520
	F2	~1850	~3200
	M1	~1640	~3720
	M2	~2000	~3370
3D post-sham	F1	~2600	~5000
	F2	~2550	~4780
	M1	~2540	~3740

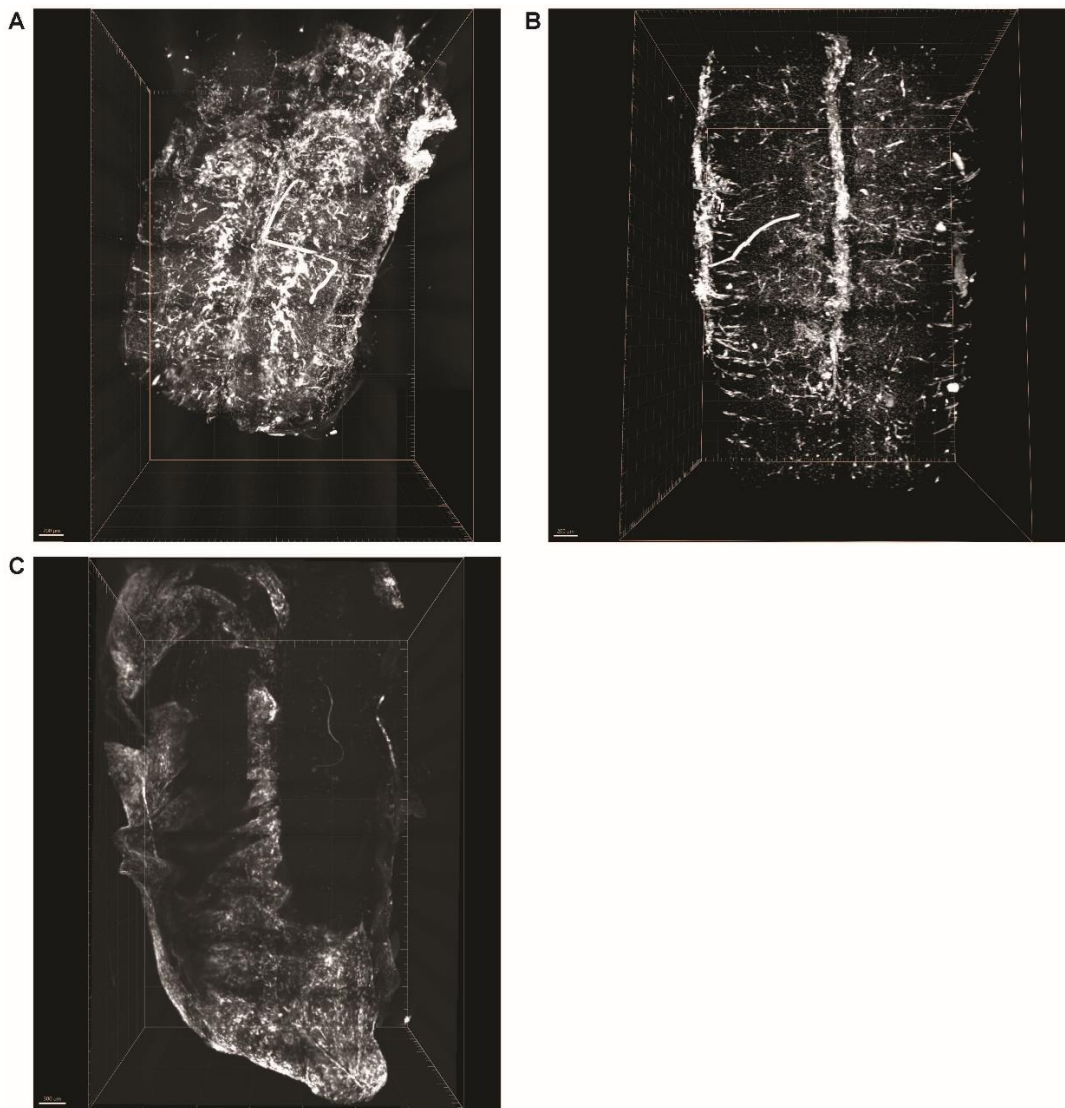


Figure C1. 3D reconstruction of mouse lumbar spinal cord of *Tmem119^{creERT2/+}; Ai14^{tdTomato/+}* mice. Coronal view showing fluorescently labeled microglia in 3 days post-SNI **A)** female and **B)** male mice. **C)** correspond to 3 days post-sham female.